l'Observatoire de Paris | LESIA

Laboratoire d'Études Spatiales et d'Instrumentation en Astrophysique

PSL UNIVERSITÉ PARIS

Wave-front Sensing & Reconstruction

Adaptive Optics Summer School
University of California, Santa Cruz

CfAO Summer School, UC Santa Cruz

Tuesday, August 20, 2019

Garima Singh

Marie-Curie Postdoctoral fellow

LESIA, Observatory of Paris, France

garima.singh@obspm.fr / guiding.honu@gmail.com

EUROPEAN COMMISSION

GS would like to thank the European Union's Horizon 2020 research and innovation programme for postdoctoral funding under the Marie Skłodowska-Curie grant agreement No 798909.

Table of Content

- Context of the talk
- Classical wavefront sensors
  - Shack-Hartmann
  - Curvature
  - Pyramid
- Wavefront reconstruction
- Extreme-Adaptive Optics for Exoplanet imaging (a high-order AO system)
  - What are the causes of residual aberrations?
  - Dedicated coronagraphic low-order wavefront sensors
    - CLOWFS / LLOWFS
  - Introduction to active speckle suppression (focal plane wavefront sensing)

Acknowledgments

- Most of the introductory notes on Shack-Hartmann and curvature wavefront sensors are taken from two books: “*Adaptive optics in Astronomy*” by Francois Roddier and *“Adaptive Optics for Astronomical Telescopes”* by John W. Hardy

- Some slides are taken from talks given by the previous lecturers of the summer school: Don Gavel, Marcos Van Dam, Richard Clare and Lisa Poyneer

- Slides on Extreme Adaptive Optics are mostly based on my professional experience in the field so far and also from the published research papers of the field referenced at the end.

- Special thanks to Faustine Cantalloube for providing information on wind driven halo and low wind effect on SPHERE.

Context of the talk: Wave-front sensing from pre-AO to post-AO regime

Adaptive Optics (AO)

Strehl ratio < 90% (current best systems like Keck/LBT/VLT) in near infrared (NIR), under good seeing

Seeing-limited → **Diffraction-limited**

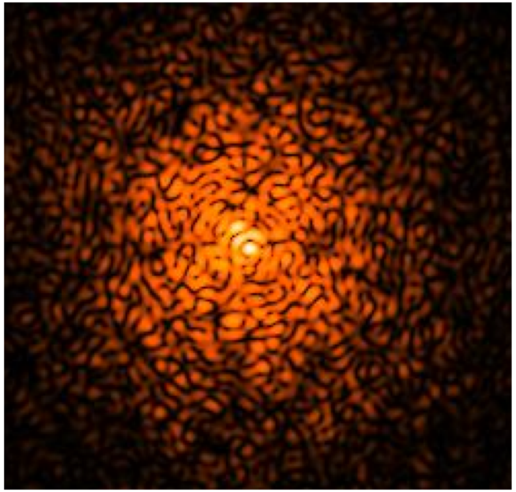

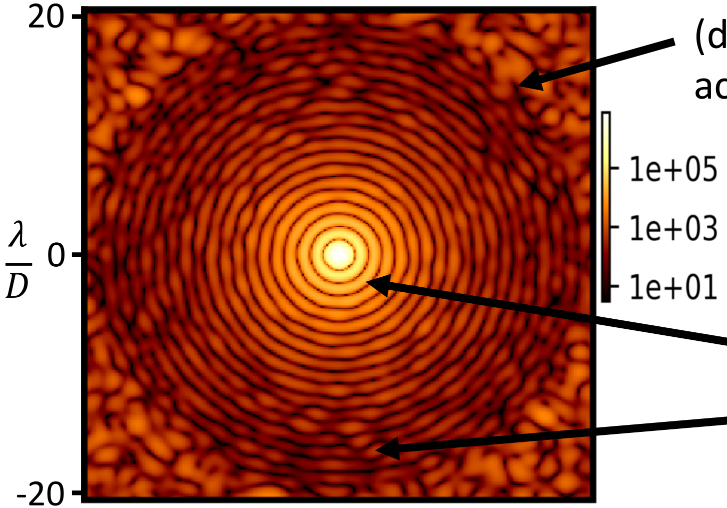

Control radius of AO (depends on the number of actuators)

PSF diffraction

Slow varying and static speckles

Simulated single short-exposure image
(PSF is not scaled with the image on right, it is just an example)

Simulated short exposure image under **post-AO residuals** seen by the SPHERE instrument at VLT for a circular pupil

Context of the talk: Wave-front sensing from pre-AO to post-AO regime

Adaptive Optics (AO)

Strehl ratio < 90% (current best systems like Keck/LBT/VLT) in near infrared (NIR), under good seeing

Extreme Adaptive Optics (Ex-AO) / High-Contrast Imaging of Exoplanets

Required Strehl ratio ~ 99% in NIR

Seeing-limited → **Diffraction-limited** → **Coronagraphic speckle suppressed image**

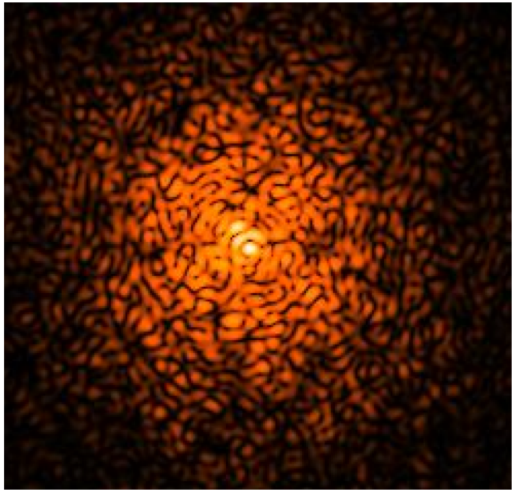

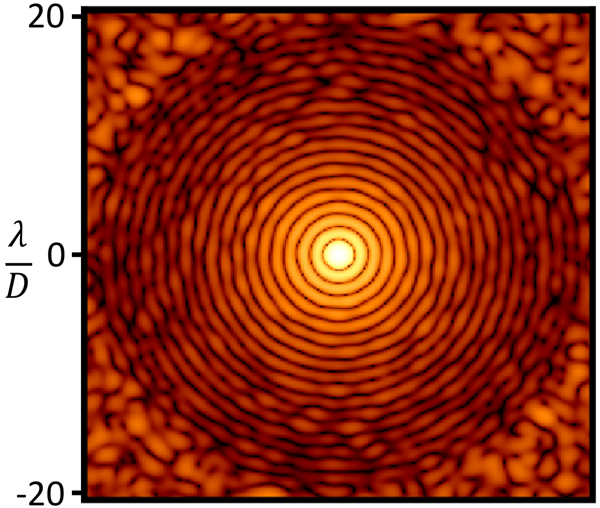

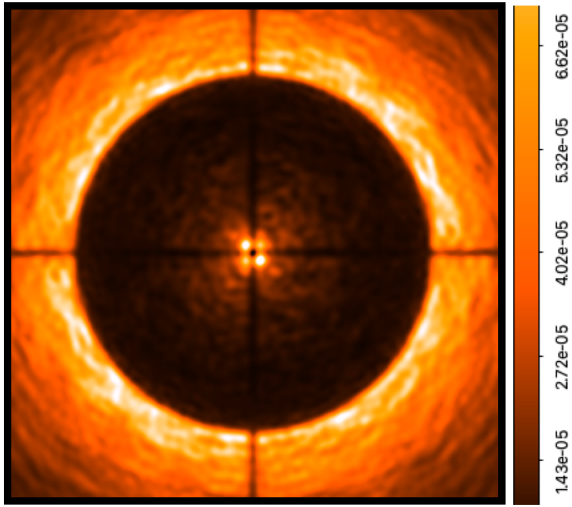

Simulated single short-exposure image

(PSF is not scaled with the images on right)

Images are not at the same brightness scale

Long-exposure simulated normalized image under SPHERE/VLT **post-AO residuals**

Wavefront Sensor: Seeing-limited to Diffraction-limited

Reminder

- ✓ Wavefront aberrations are random. Described using statistical estimates such as variances, or covariances.

- ✓ Waves are described as a complex number $\Psi = \mathrm{A}e^{i\phi}$, A and ϕ are real numbers representing the amplitude and phase of the fluctuating field.

- ✓ Instead of an absolute phase measurement, we measure the difference between the phase $\phi(x)$ at a point x and phase $\phi(x+\xi)$ at a near by point at a distance ξ on the telescope aperture.

- ✓ The root mean square (rms) phase distortion over a circular area of diameter r_0 is about 1 radian. Phase perturbations with amplitude ≤ 1 radian have little effects on the image quality (except for the exoplanet imaging application of AO).

- ✓ Image quality degrades exponentially with the variance of the wave-front distortion.

- ✓ Most wavefront sensors (WFS) measure the ***direction of propagation*** of the optical wavefront (WF) rather than its optical phase. WF reference sources emit incoherent radiation, thus absolute measurements of optical phase is not possible.

- ✓ Phase information is translated into intensity signals.

Two ways of sensing

Pupil plane techniques

Interferometry

For ex: "Shearing interferometer"

Beam superposition to form interference fringes coding the phase difference between the two beams

Geometrical Optics concept

For ex: "Shack Hartmann/ Curvature sensing"

Determine the angle of arrival of the rays i.e. local slope or curvature of the WF

Focal plane techniques

For ex: "Phase Diversity"

- Derive phase directly from the intensity distribution in the focal plane through Fourier transform. No phase reconstruction is required!
- Spatial Invariance: intensity variations in image plane not directly related to specific locations in pupil plane
- Computation intensive, doesn't work when aberrations are large

Wavefront Sensor: Measuring local gradients/slopes

✓A random WF error over a 2D aperture can be specified as Zonal or Modal.

✓**Zonal:** Aperture is divided into an array of independent subapertures or zones. WF is expressed in terms of the Optical Path Difference (OPD) over these spatial zones.

Wavefront

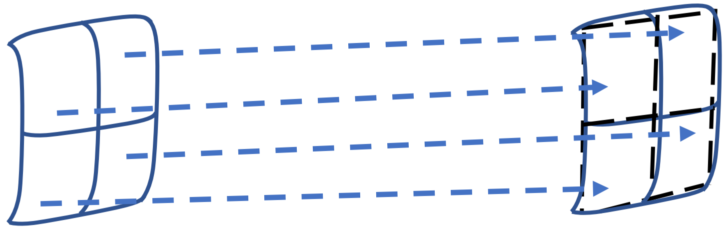

WFS measures the WF gradients or curvature within the array of zones covering the telescope aperture.

✓**Modal:** When the WF is expressed in terms of coefficients of the modes of a polynomial expansion over the entire pupil, for example, Zernike polynomials for a circular aperture.

Wavefront

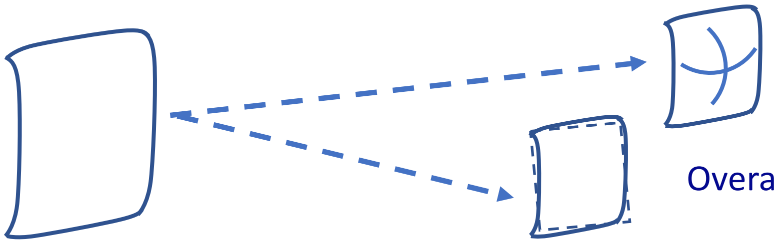

Astigmatism

Overall tilt

WF is decomposed into distinct surface shapes for example overall tilt, astigmatism and defocus etc

Wavefront Sensor: Seeing-limited to Diffraction-limited

A WFS is composed of three main components:

- **Optical device**
  Transforms the WF aberrations into the light intensity variations.
- **Light detector**
  Transforms the light intensity into electrical signal.
- **Wave-front reconstruction**
  Convert the signals into phase aberrations or WF sensor measurements into DM commands.

Requirements of a WFS*:

- **Quality of Measurement**
  Sensitivity and accuracy specified in terms of fractions of waves λ/X where X may be between 10 and 20
- **Limiting Magnitude**
  Must work on faint objects. Require detectors with high quantum efficiency and low noise.
- **Incoherent sources**
  Must work with white light incoherent point/extended sources.
- **Must have large linear range. Should be able to measure large WF errors**

* Not an exhaustive list

Wavefront Sensor: Measuring local gradients/slopes

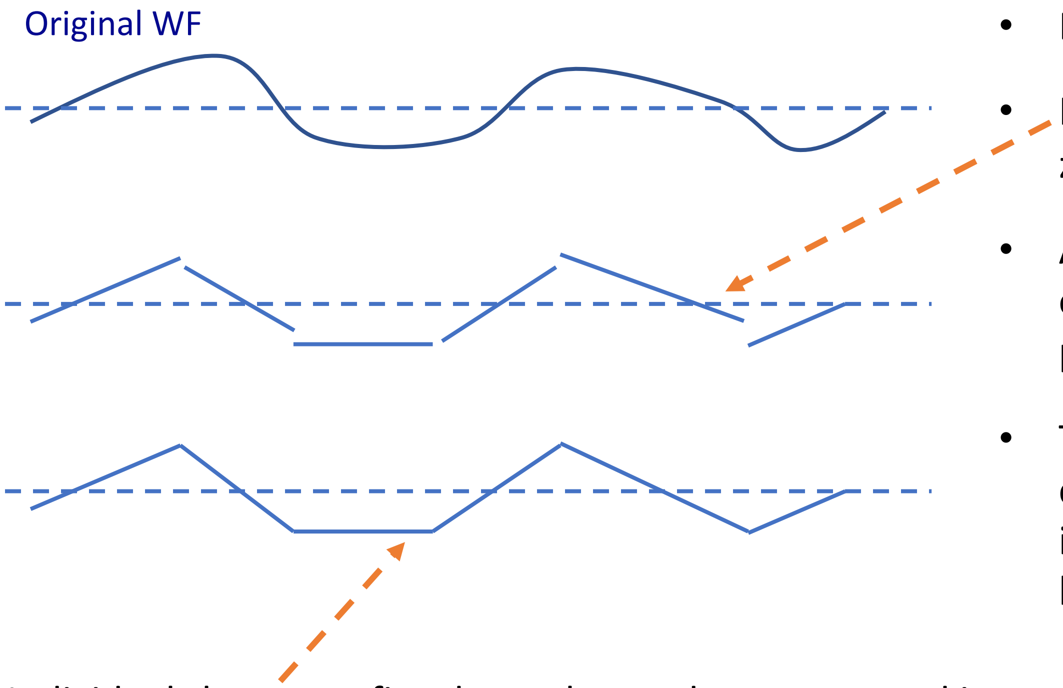

- Divide the aperture into zones/subapertures
- Image the reference source within each such zone
- Average WF slope is simultaneously measured over each zone. Note that the relative phase or piston component of each subaperture is lost.
- Technically, the WF slopes in each zone can be corrected individually, however, would result in incoherent superposition of the images formed by each zone. Thus, loss in angular resolution.

Individual slopes are fitted together and reconstructed into a continuous surface that best fits the measured data (i.e. minimizing the mean-square errors between the reconstructed wf and the measured gradients).

Shack Hartmann WFS and shearing interferometer are based on this principle.

Wavefront Sensor: Measuring local gradients/slopes

Shack-Hartmann WFS: Measures the spatial first derivative i.e. the gradient of the wavefront (a Zonal WFS).

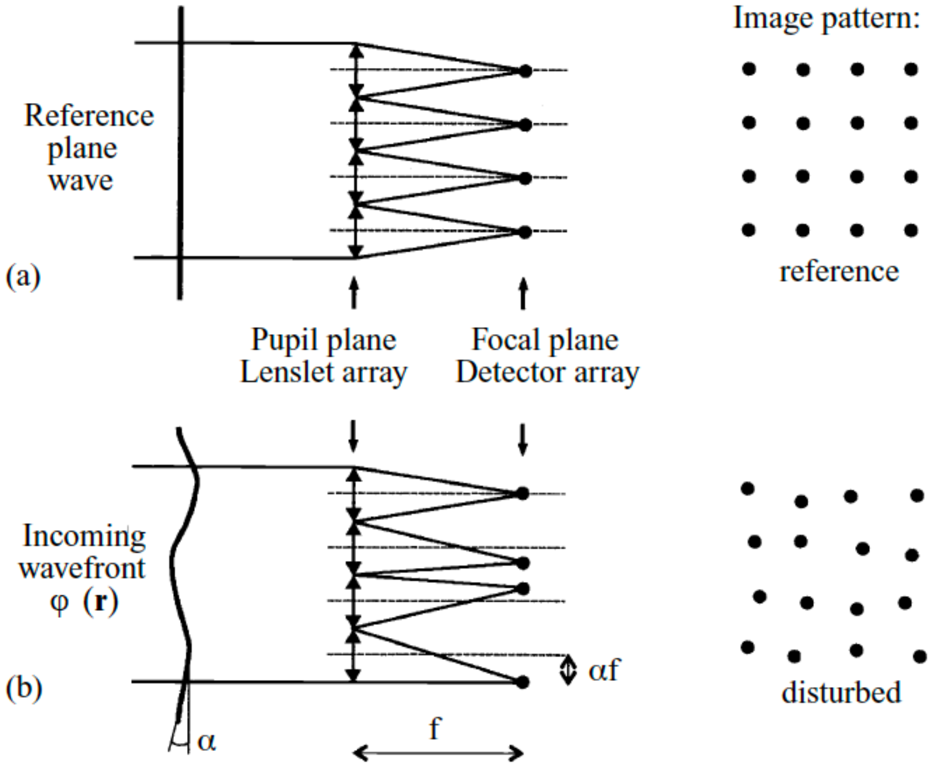

- A lenslet array is placed in a conjugate pupil plane to sample the incoming WF.
- Measurement of the image position gives a direct estimate of the angle of arrival of wave over each lenslet.
- Each lenslet create a map of local WF slope.
- Need to calibrate the focus positions of the lenslet array.

Figure reference: *"Adaptive optics in Astronomy" by Francois Roddier*

Spot size/subaperture size

The spot size is determined by 4 factors: the subaperture dimension d, the angular diameter of the source θ, the turbulence strength r_0, and the sensor wavelength λ

- d is on the order of the actuator pitch (often exactly the actuator pitch– Fried geometry), and is on the order of r_0 at the science wavelength

- r_0>d, angular size of the spot is $\sim\lambda$/d.

- r_0 <d, image of an unresolved source is determined by r_0 ($\sim\lambda$/ r_0)

- Bigger subapertures means more light and better SNR in centroid measurement. However, poorer fit to WF.

- Smaller the aperture, the more accurately a WF can be measured. If subapertures are too small, spot size increases due to diffraction, which degrades spot centroid estimate. Subaperture must be large enough to resolve the isoplanatic patch.

- WF variations < subaperture size can not be measured. Slope sensor acts as a low-pass filter!

How to measure the position of spots?

A CCD to record all the images simultaneously

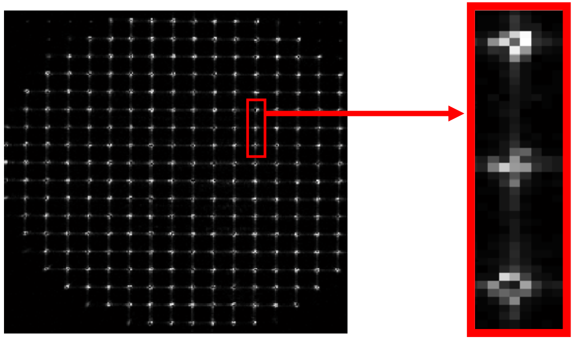

4 x 4 pixels or more

Estimate center of gravity position (c_x, c_y)

$$c_x = \frac{\sum_{i,j} x_{i,j} I_{i,j}}{\sum_{i,j} I_{i,j}} \text{ and } c_y = \frac{\sum_{i,j} y_{i,j} I_{i,j}}{\sum_{i,j} I_{i,j}}$$

$I_{i,j}$ and ($x_{i,j}$, $y_{i,j}$) are the signals and the position coordinates of the CCD pixel (i,j).

A four quadrant detector (quad-cell) for each subaperture

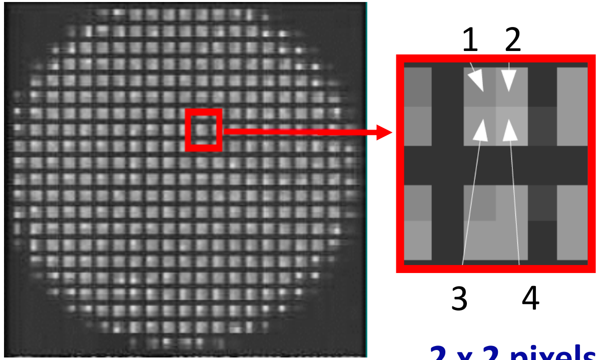

2 x 2 pixels

Measured angle of arrival could be estimated as

$$\alpha_x = \frac{\theta_b}{2} \frac{I_1 + I_2 - I_3 - I_4}{I_1 + I_2 + I_3 + I_4}$$

Spot size (angular size on sky)

Measurement error with SHWFS

- Random errors in determining the positions of the spots due to photon noise and electronic noise (dark current/read out) in the detector
- Bias errors due to misalignment of the optics

Table 5.2. *Noise behaviour for the Shack–Hartmann*

	Photon noise SNR in subaperture = $n_{ph}^{-1/2}$		Electronic noise SNR in subaperture $= n_{ph}/n_{bg}^{-1/2}$	
	Diffraction-limited	Seeing-limited	Diffraction-limited	Seeing-limited
σ_s	$n_{ph}^{-1/2}$	$n_{ph}^{-1/2}(d/r_0)$	$\sigma_e N_D n_{ph}^{-1}$	$\sigma_e N_D n_{ph}^{-1}(d/r_0)^2$

Number of photoelectrons from the sky background distributed over windowed FOV.

Measurement noise variance

Number of photoelectrons per subaperture and exposure time

rms of noise electrons per pixel and per frame (noise due to read out and dark current)

FWHM of subaperture's diffraction pattern

$$\boldsymbol{\sigma_s \propto 1/(SNR^2)}$$

Table reference: *"Adaptive optics in Astronomy"* by Francois Roddier

How to measure the position of spots?

A CCD to record all the images simultaneously.	A four quadrant detector (quad-cell) for each subaperture

A CCD to record all the images simultaneously.

- Better linearity with small pixels size
- Dynamic range may be increased by using pixels of large size. There is no crossover between the subapertures, however, it lets in more sky background.
- More pixels on a subaperture means noisier estimation of the centroid due to read noise/dark current. Noise can be reduced by windowing the centroid. Windowing is used to eliminate the background around the central core of the image.

A four quadrant detector (quad-cell) for each subaperture

- The image size must be known!

If images are diffraction-limited, $\theta_b = \frac{\lambda}{d}$

If seeing-limited, $\theta_b \sim \frac{\lambda}{r_0}$, spot size depends on seeing conditions and is unknown.

- Quad-cell response can not be pre-calibrated!
- Centroid is linear with displacement over a small region (limited dynamic range). Could defocus the source image to a known spot size but at the cost of SNR
- Faster to read and compute centroid, less sensitive to noise

Quad-cell presents larger error due to photon noise than the center of gravity approach, similar sensitivity to sky background noise and a smaller error due to detector noise

Advantages of a SHWFS

- SHWFS is achromatic because the OPD in turbulence is achromatic, hence works with broadband white light
- Can operate with extended sources if the FOV is adapted to the source size
- Linear with large dynamic range (when using a CCD)

Drawbacks of a SHWFS

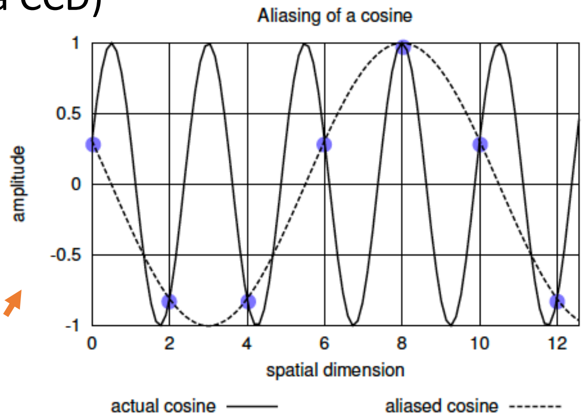

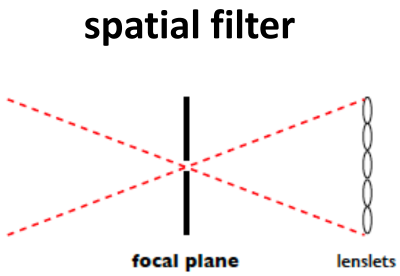

- Misalignment problems
- Calibration precision
- Could be drift sensitive
- Aliasing errors: High frequency errors incorrectly measured as low-frequency errors! A spatial filter (a field stop of width λ/d in focal plane) can be used to overcome it.

It's a widely used sensor in Astronomy (Hale Telescope, Gemini South, Very Large Telescope), Ophthalmic applications, improving retinal imaging and mapping the aberrations of the eye (Dreher et al. 1989).

Wavefront Sensor: Measuring local curvatures (Roddier 1987)

Curvature WFS: Measures the second derivative of the phase i.e. its Laplacian (a Modal WFS!)

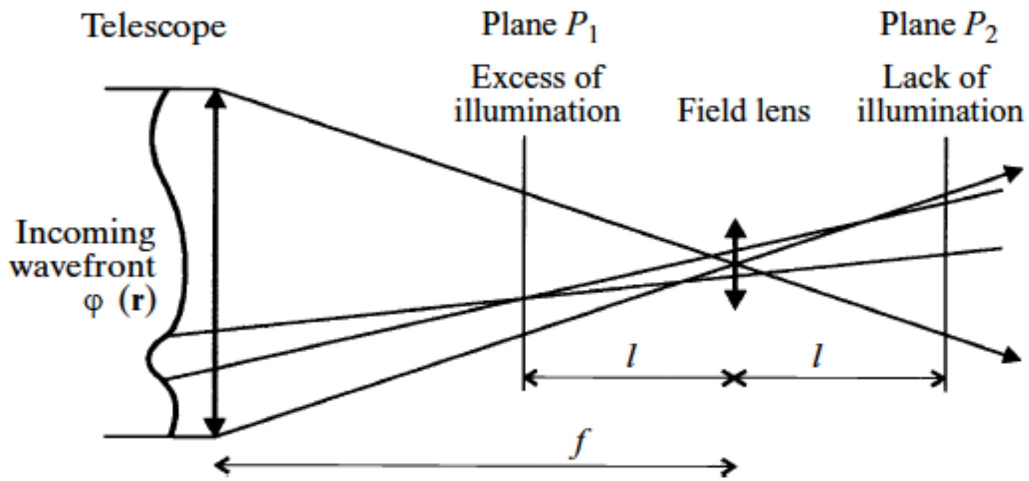

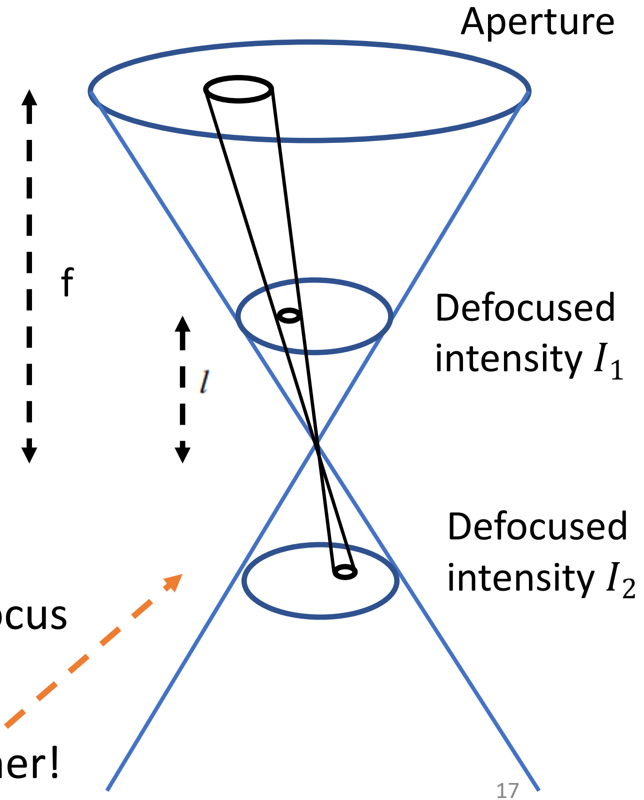

- Records the irradiance distribution at distance $\pm l$ from the focus
- A local WF curvature in the pupil produces an access of illumination in one plane and a lack of illumination in the other!

Figure reference: “*Adaptive optics in Astronomy*” *by Francois Roddier*

$$\frac{I_1(\mathbf{r}) - I_2(-\mathbf{r})}{I_1(\mathbf{r}) + I_2(-\mathbf{r})} = \frac{\lambda f(f-l)}{2\pi l}\left[\frac{\partial \varphi}{\partial n}\left(\frac{f\mathbf{r}}{l}\right)\delta_c - \nabla^2\varphi\left(\frac{f\mathbf{r}}{l}\right)\right], \tag{5.10}$$

Normalized difference between the irradiance distributions measured in planes P_1 and P_2

WF radial first derivative at the edge of the beam

measurement of the local WF curvature inside the beam

Choice of l is very important in curvature sensing!

The blur produced at defocused pupil planes ($(f-l)\theta_b$) should be **<** size of the WF fluctuations to be measured (to avoid smearing of the intensity variations) or the areas over which the curvature is to be measured ($l\,d/f$) and,

The size of the WF fluctuations is the subaperture size!

Equation reference: "*Adaptive optics in Astronomy*" by *Francois Roddier*

Point source, d > r_0

$$l \geqslant \frac{\lambda f^2}{r_0 d}.$$

- Blur angle is given by $\theta_b = \lambda / r_0$
- Only low-order aberrations are measured!

Point source, d < r_0

$$l \geqslant \frac{\lambda f^2}{d^2}.$$

- High-order aberrations of spatial scale d are measured!

- Sensitivity of the sensor is inversely proportional to the defocusing!
- Increasing the distance increases spatial resolution on the WF measurement but decreases sensitivity.
- A smaller distance yields a higher sensitivity to low-order aberrations. Smaller distance reduces the aliasing error. Also reduces measurement noise.
- l is typically in the range of 1-20 cm. Sensitivity and dynamics are easily adjusted by the distance l.

- Curvature sensor works very well with incoherent white light.

- Curvature is a scalar field and requires one value per point! Thus intensity in each subaperture is measured with a photon counting avalanche photodiodes without readout noise. Its cost effective!

- The photon error in a single subaperture of a curvature sensor is similar in magnitude to that of an equivalent SHWFS tilt sensor. However the error propagation in the reconstruction process is greater than the SHWFS (will discuss more later).

- It is also possible to use the curvature sensor signal to directly drive a corrective element (such as a bimorph or membrane mirror). Faster and less computationally expensive than performing a full reconstruction.

- Subaru Telescope AO188 system has a curvature sensor.

Wavefront Sensor: Pyramid WFS (PS, R. Ragazzoni)

Concept based on the Foucault knife edge test

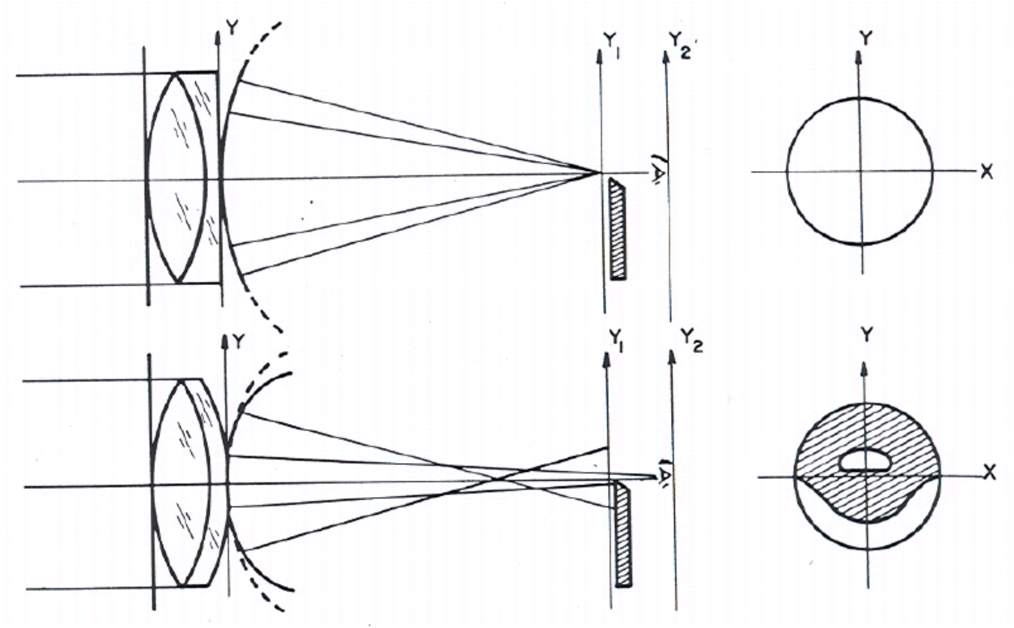

Knife edge test for perfect lens (top), and one with spherical aberration (bottom). At right are observer views of pupil in each case.

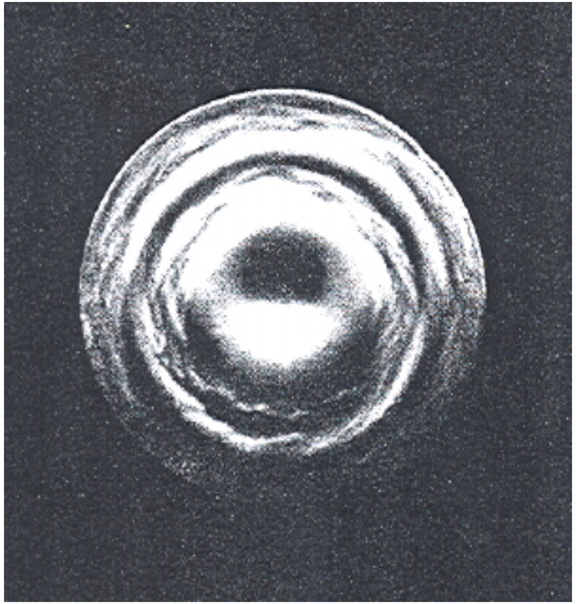

An irregular mirror tested with knife-edge test

Sorting of the rays in the focal plane by the Knife edge test for an aberrated lens

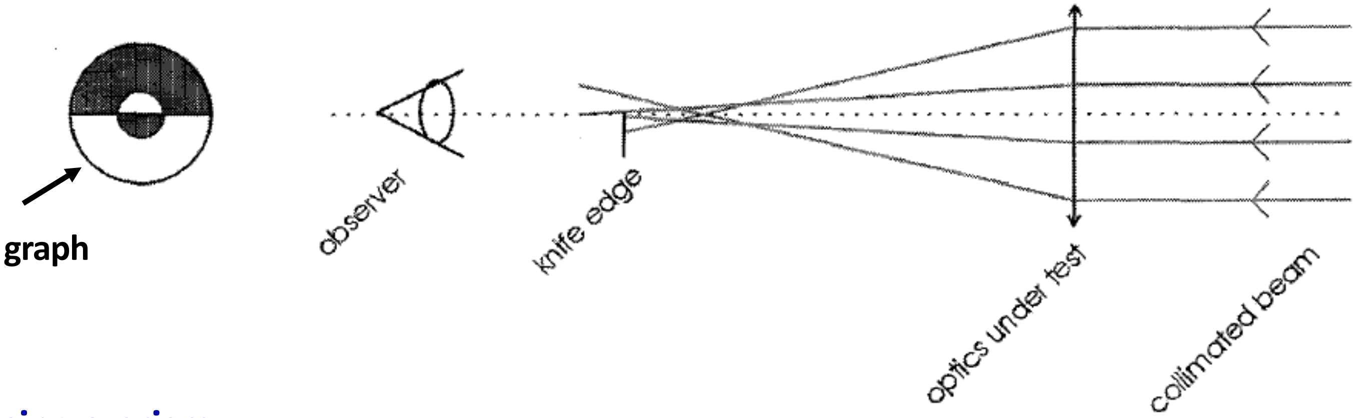

Foucault graph

1D PS using a prism

Sum of the lower and upper pupil is a constant

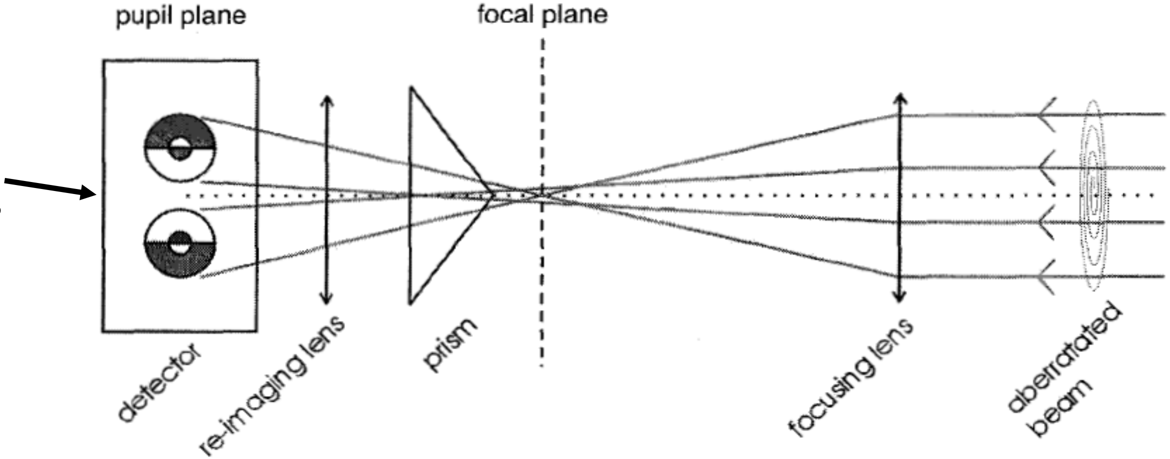

Reference: https://dspace.library.uvic.ca/bitstream/handle/1828/604/ledue_2005.pdf?sequence=1

Wavefront Sensor: PS

- Simultaneous implementation of four Foucault knife-edge measurements.
- PS splits the focal plane in four quadrants, which are imaged by a relay optics onto the pupil plane, producing four images of the pupil.

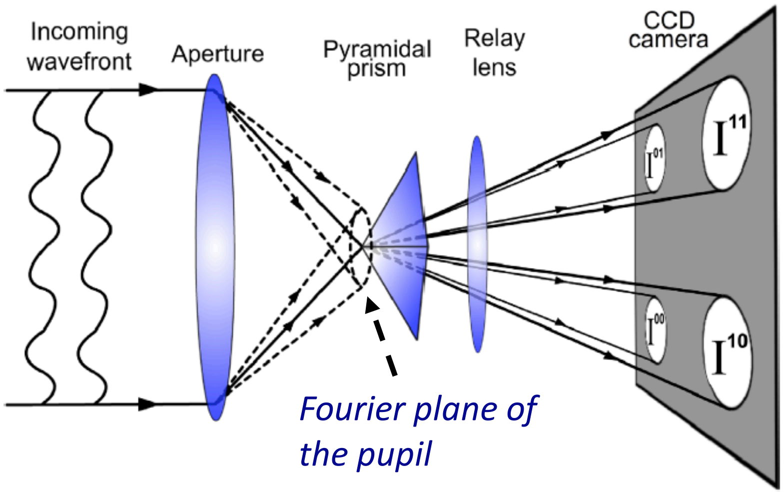

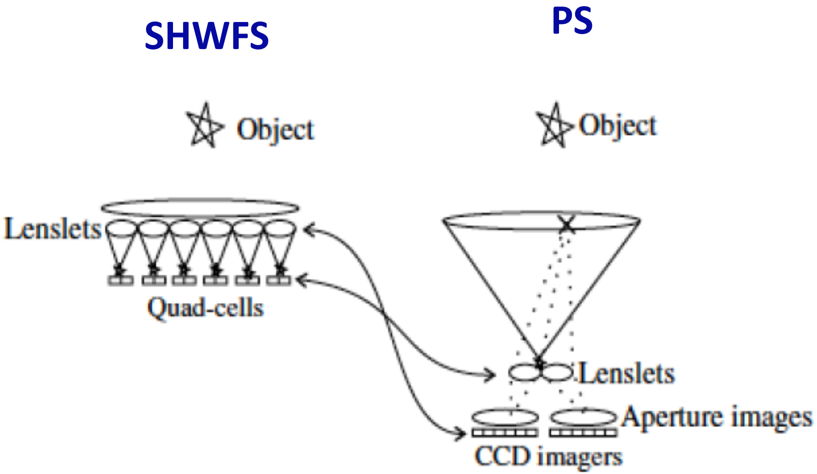

- If the system is un-aberrated and the effects of diffraction are ignored, then the 4 pupil images should be identical.

Figure reference: Hutterer et al 2019

Figure reference: Chew et al 2006

Wavefront Sensor: PS

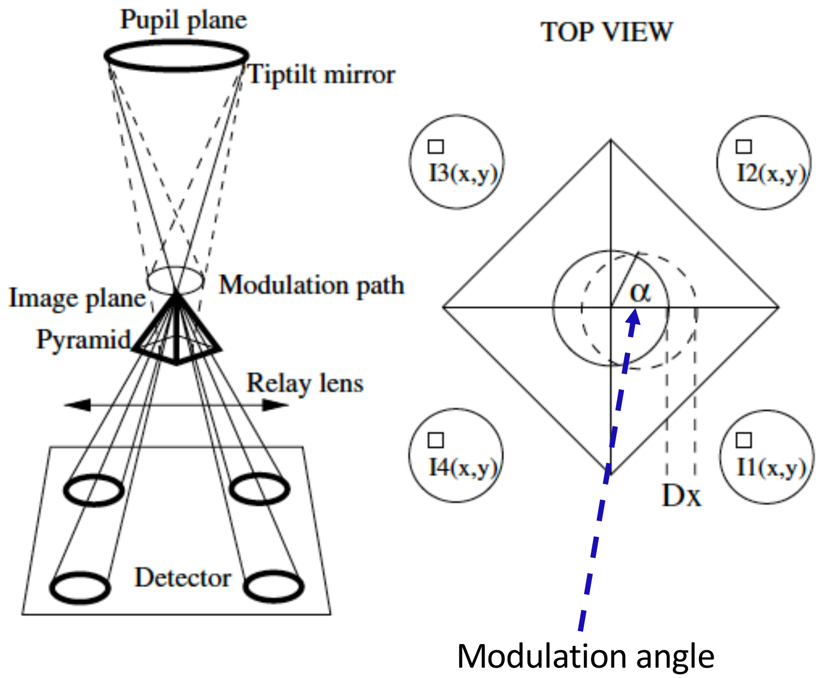

- If wavefront slope is large, all the incoming light will fall only on one facet of the pyramid. Signal will then be independent of the gradient modulus and the corresponding detector area will saturate. Produce highly non-linear response.
- To avoid this, oscillate or modulate the pyramid.
- The signal for each subaperture is given by

$$S_x(x,y) = [(I_1(x,y) + I_2(x,y)) - (I_3(x,y) + I_4(x,y))]/I_0,$$
$$S_y(x,y) = [(I_1(x,y) + I_4(x,y)) - (I_2(x,y) + I_3(x,y))]/I_0,$$

$$\sin(S_x) \simeq S_x = \frac{\lambda}{\alpha\pi^2}\frac{\mathrm{d}\phi}{\mathrm{d}x}$$

Sensitivity ∝ 1/α for small aberrations. PS acts as a slope sensor for very low-order modes and large α

- $I_i(x,y)$ is the intensity in the subaperture located at (x,y) in the quadrant *i*. Intensities are integrated during a modulation cycle. I_0 is the average intensity per subaperture.

Figure reference: “On the nature of the measurements provided by a pyramid Wavefront sensor”. Christophe Verinaud, Optics communications 233 (2004)

SHWFS vs PS

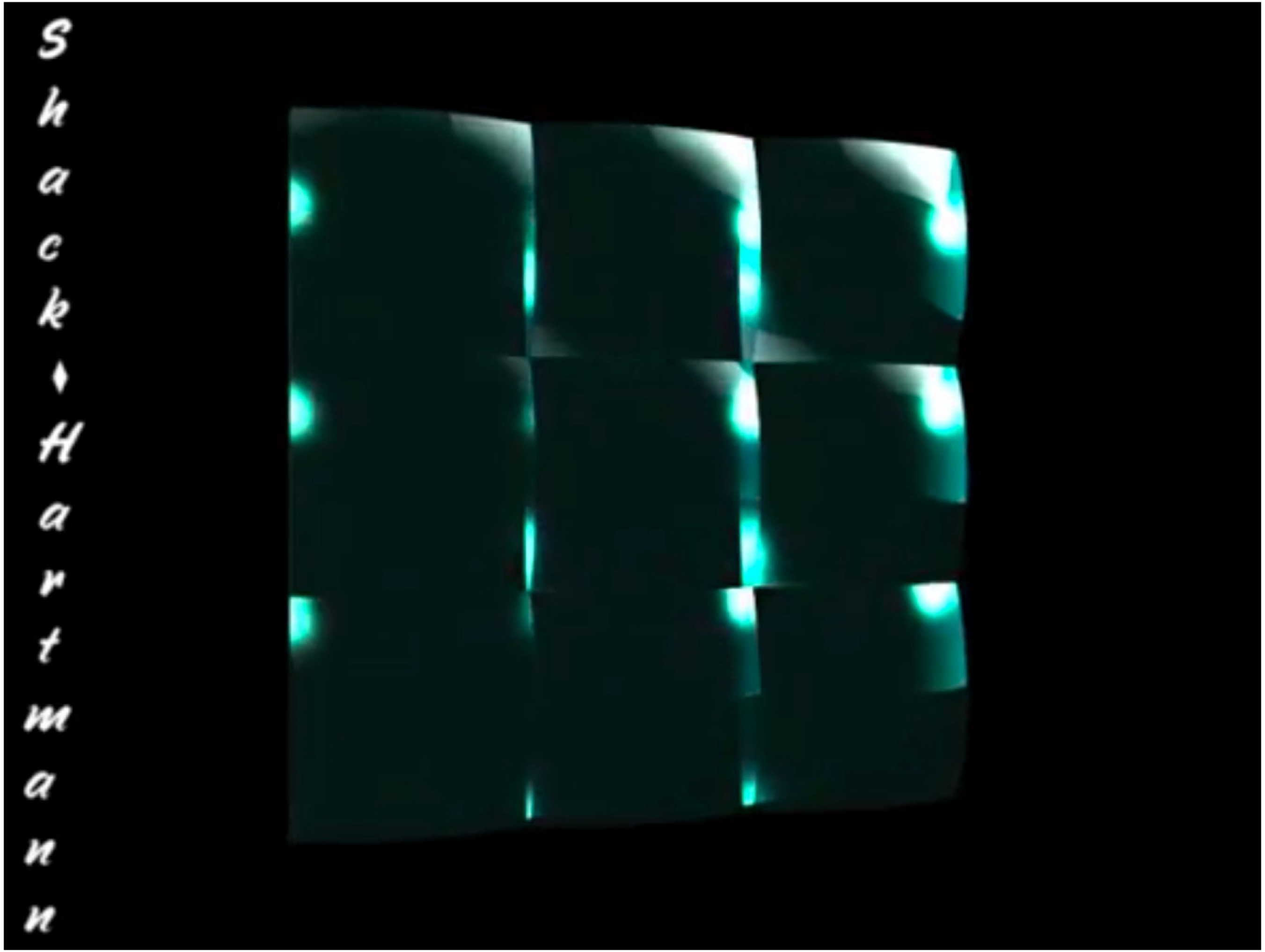

PS provides better sensitivity than the SHWFS!

* As WF slopes becomes small, PS becomes a phase-type sensor!

https://www.youtube.com/user/PadovAdOpt/videos

Wavefront Reconstruction

How to determine the WF phase from a map of its gradient or Laplacian?

The shape of the wf is found by spatially integrating the individual zonal gradients/curvature measurements over the whole aperture. The reconstructed map is sampled at an interval equal to the subaperture size!

Let's say S is a measurement vector of M elements of slopes in two directions.
ϕ, a vector of N commands or N phase values over a grid which is unknown.

$$\boldsymbol{\phi} = \boldsymbol{BS}$$

B is a reconstruction matrix (or command matrix, a matrix from centroids to actuators).

How to derive matrix *B*? … an inverse problem!

Two methods: the zonal method and the modal method

Wavefront Reconstruction: zonal matrix method (Basis set is the actuators)

Link measurements S to the incoming phase ϕ $\quad$ $\boldsymbol{S = A\,\phi}$

Consider a SHWFS with square subapertures. Assume Fried geometry between subapertures and actuators.

Fried geometry

Actuators
Subapertures

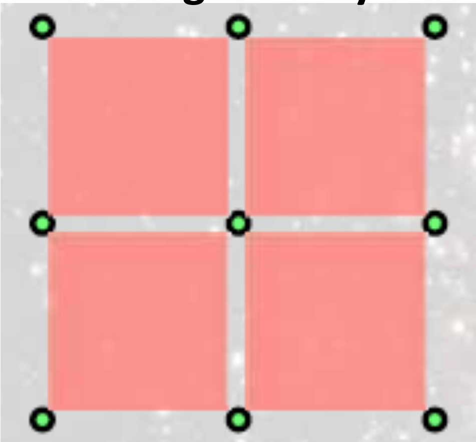

$$\mathbf{S}^x_{i,j} = [(\phi_{i+1,j+1} + \phi_{i+1,j}) - (\phi_{i,j} + \phi_{i,j+1})]/2d$$

$$\mathbf{S}^y_{i,j} = [(\phi_{i+1,j+1} + \phi_{i,j+1}) - (\phi_{i,j} + \phi_{i+1,j})]/2d,$$

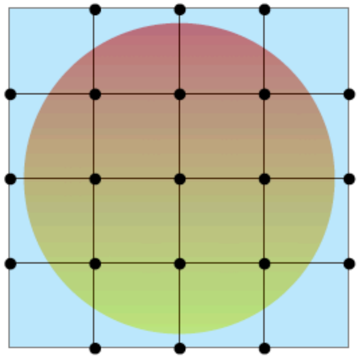

Phase in pupil

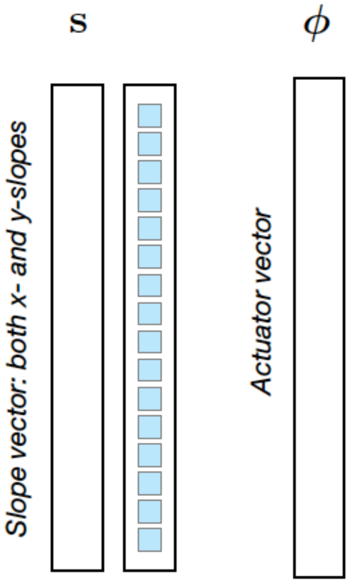

ϕ's are the phase values at the four corners of a subaperture. S are the corresponding measured slopes.

Wavefront Reconstruction: zonal matrix method

How to make sure we have the right registration?

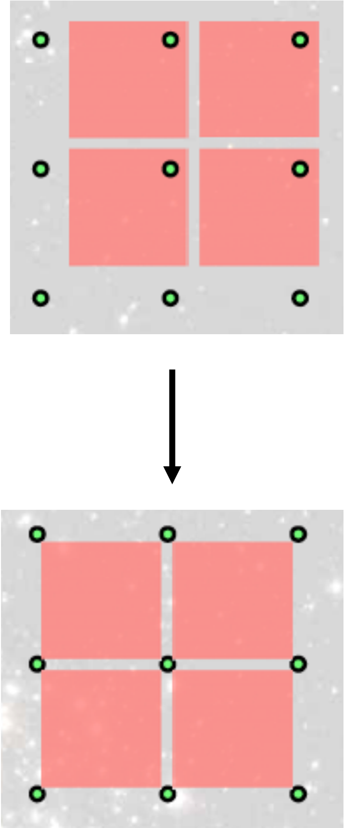

Add waffle to the DM and adjust lenslet array or the beam until no centroids are measured

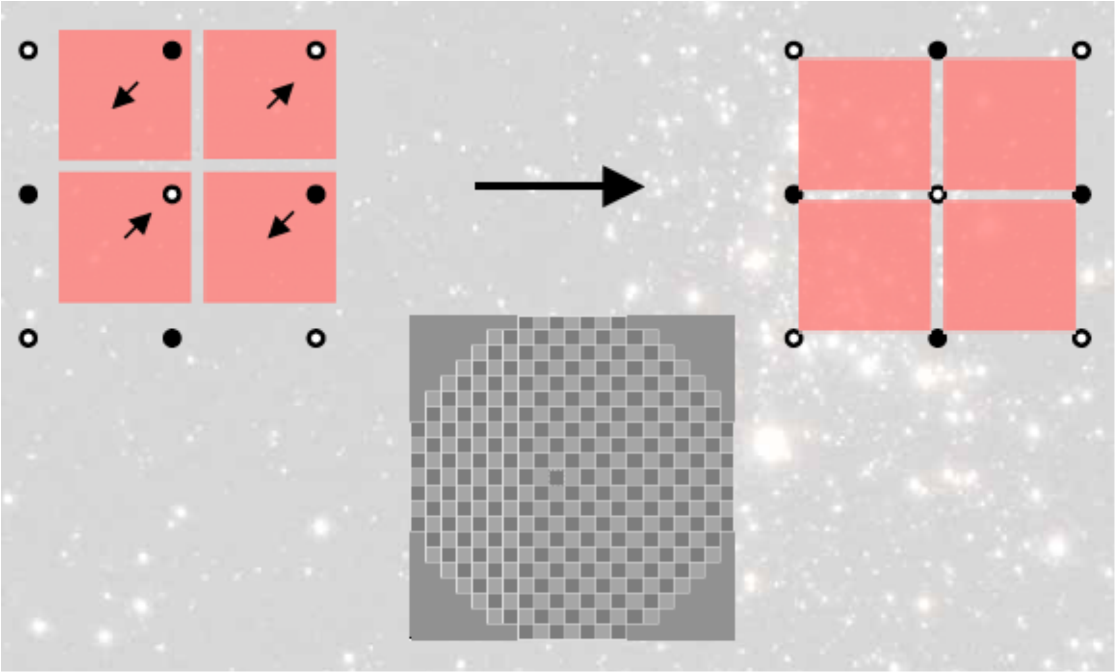

Wavefront Reconstruction: zonal matrix method

An interaction matrix ***A*** describes how a signal applied to the actuators ($\boldsymbol{\phi}$), affects the centroids, ***S***

$$\boldsymbol{S = A\ \phi + n}$$

Apply unitary voltages to each actuators (keeping all the others to 0) and record the response of the sensor.

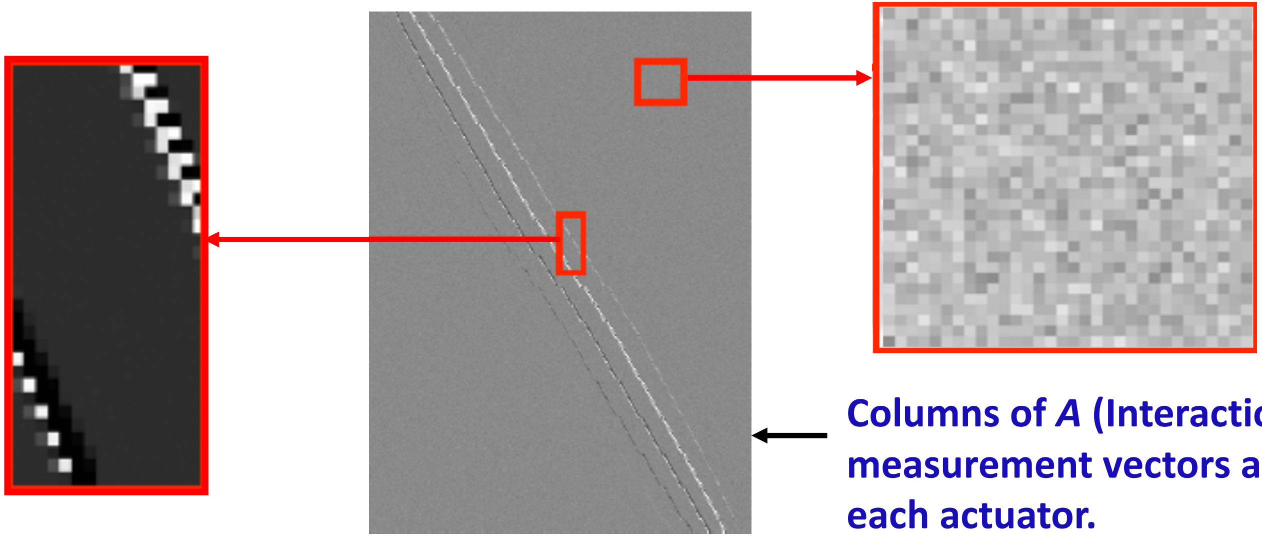

***n*, Noise of zero mean**

Columns of *A* (Interaction matrix) are the measurement vectors associated with each actuator.

***A* maps actuators to sensors.**

Wavefront Reconstruction: zonal matrix method

We have an interaction matrix, $S = A\,\phi$

We need a reconstruction matrix to convert from centroids to actuator voltages $\phi = BS$

$$A\,\phi = S$$

$$A^T A\,\phi = A^T S$$

$$\phi = \underbrace{(A^T A)^{-1} A^T}_{\text{Least square reconstructor, } B} S$$

$(A^T A)^{-1}$ is not invertible because modes such as waffle and piston are invisible.

Pseudo- inverse of A is calculated via Singular value decomposition!

Measurement error is then $\epsilon_S = \|\mathbf{S} - \mathbf{A}\boldsymbol{\phi}\|^2$

WF error ϕ is estimated so that ϵ_S is minimized in a closed-loop operation.

Mini break: Brief questions?

* Haven’t discussed noise propagation in WF reconstruction, Modal/Fourier reconstruction methods

Extreme AO: Diffraction-limited to Coronagraphic speckle suppressed image

Strehl ratio and residual WF errors are two main parameters that differentiate AO from an ExAO system. A typical SR of ~40% with 150 nm RMS of total phase residual is sufficient to obtain a diffraction-limited PSF at near-IR wavelengths.

However, an ExAO system requires SR > 90% and total phase residuals of < 10 nm RMS!

- Extreme-Adaptive Optics (ExAO) for Exoplanet imaging
  - Concept of direct imaging of exoplanets
  - What causes residual aberrations?
  - Dedicated coronagraphic low-order wavefront sensors
  - Introduction to active speckle suppression (focal plane wavefront sensing)

Concept of direct imaging of Exoplanets

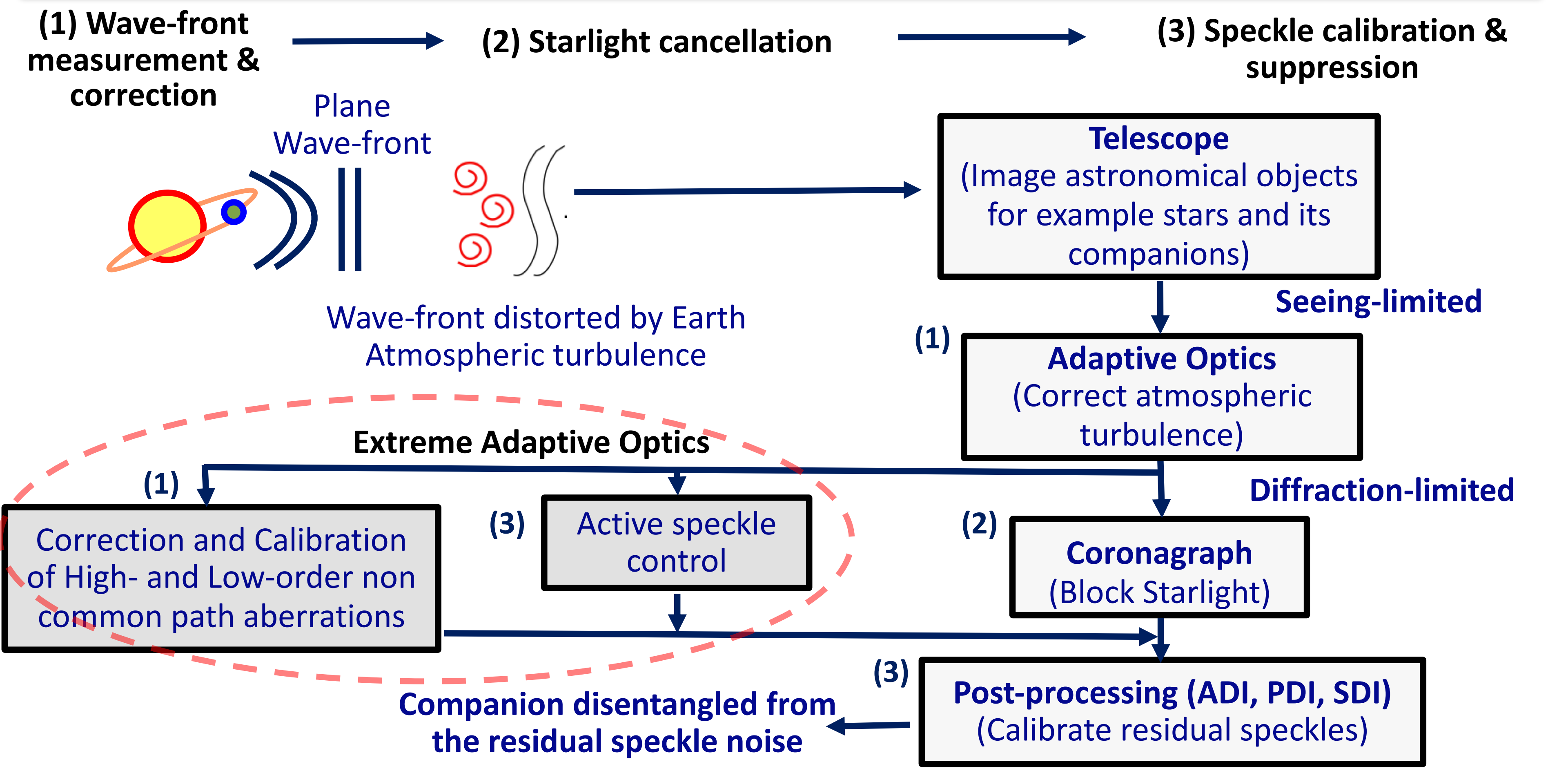

What causes residual aberrations in Exoplanet Imaging?

Low-order aberrations

Causes: Temperature variations, thermal distortions, optical/mechanical vibrations, alignment errors due to telescope motors and chromatic errors.

Effects: Starlight leak around a coronagraphic mask, prevent detection at small angles.

Non-common path aberrations (NCPA)

Cause: different AO sensing and science imaging channels.

Effects: Evolving quasi-static stellar speckles, which not only mask faint exoplanet signals but also create false positive signals.

Low-wind effect

Cause: Spider arms of the secondary can cool below the ambient air temperature due to radiative losses. Change in air index from one side of the spider to the other.

Effects: Each quarter of the pupil shows different piston and sometimes tip-tilt phase errors.

Wind driven halo

Cause: High wind speeds at the upper level of turbulence across the pupil moving faster then the speed of AO loop correction.

Effects: A typical butterfly-shaped structure in the focal plane image along the wind direction.

Concept of starlight cancellation: Stellar Coronagraphy

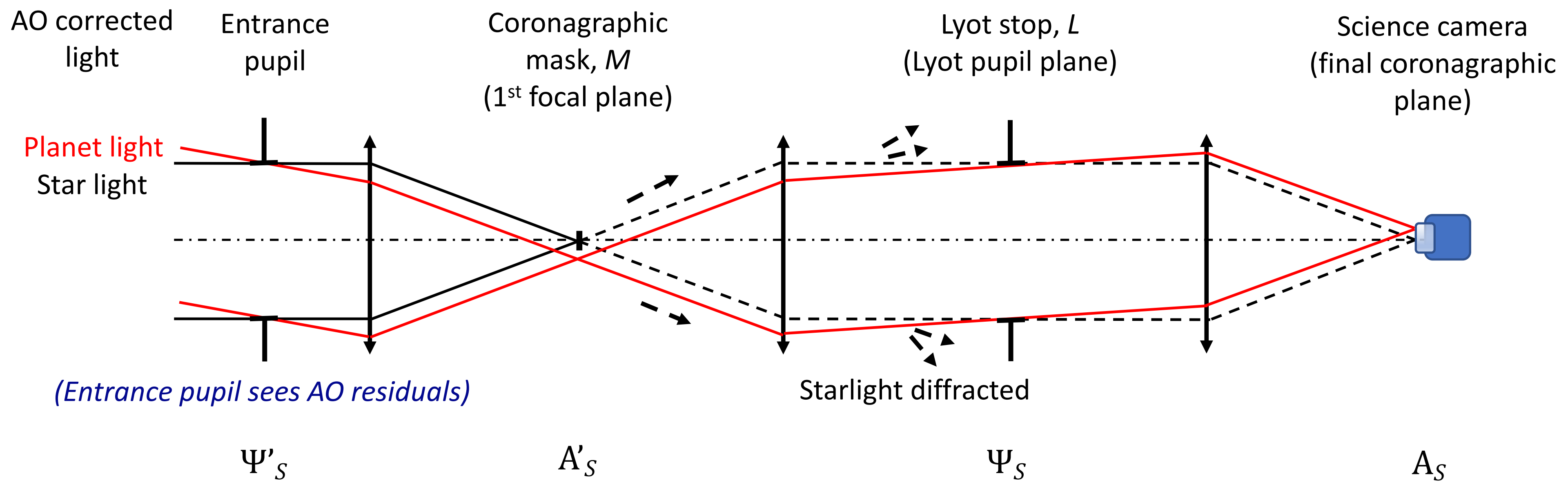

Fraunhofer approximation is considered to explain the effects of diffraction between the pupil and focal planes.

Fourier transform ($\mathcal{F}$) is used to analyze the complex amplitude of the field from focal to the pupil plane and the inverse Fourier transform ($\mathcal{F}^{-1}$) from pupil to the focal plane.

Concept of starlight cancellation: Stellar Coronagraphy

Assuming star is a spatially unresolved monochromatic source centered on the optical axis.
The complex amplitude of the star in the entrance pupil plane is

$$\psi'_S(\xi, \lambda) = \psi_0 P(\xi) \exp(\mathrm{i}\Phi(\xi)),$$

P = Entrance pupil, ψ_0 = mean amplitude of field over *P*, ξ = pupil coordinate

Assuming small aberrations (<< 1 radian RMS),

$$\frac{\psi'_S(\xi, \lambda)}{\psi_0} \simeq P(\xi) + \mathrm{i}\Phi(\xi). \qquad \text{Eq 1}$$

The complex amplitude of the electric field A'_S behind the coronagraphic mask *M* in the first focal plane is,

$$A'_S = \mathcal{F}[\psi'_S]\, M, \qquad \text{Eq 2}$$

where $\mathcal{F}$ is the Fourier Transform.

The electric field ($\Psi_S = \mathcal{F}^{-1}(A'_S)$) at the corresponding Lyot pupil plane can be written as:

$$\frac{\mathcal{F}^{-1}[A'_S]}{\psi_0} = P * \mathcal{F}^{-1}[M] + \mathrm{i}\Phi * \mathcal{F}^{-1}[M], \qquad \text{Eq 3}$$

* is the convolution product.

Multiply the electric field Ψ_S with a Lyot stop (L). The electric field can then be written as:

$$\frac{\psi_S}{\psi_0} = (P * \mathcal{F}^{-1}[M])L + (\Phi * \mathcal{F}^{-1}[M])L$$ Eq 4

Consider a perfect coronagraph without any manufacturing defects, the starlight is centered at *M* and is rejected completely outside of the geometrical pupil. The first term in Eq 4 can be equated to 0 analytically.

In the final focal plane, the complex amplitude A_S is the Fourier transformation of the field after the Lyot stop.

$$A_S = i\psi_0(\mathcal{F}[\Phi]M) * \mathcal{F}[L]$$ Eq 5

The intensity at the coronagraphic plane is $I = |A_S|^2$

Important result!

Complex amplitude at the final focal plane is directly linked to the wave front aberration in the pupil plane (Eq 5). If we can measure A_S, we can directly retrieve the wavefront errors! This is useful to actively suppress speckles.

(See slide 57 to know how to measure the phase errors from the focal plane complex amplitude)

Concept of starlight cancellation: Stellar Coronagraphy

*images are not at same brightness scale

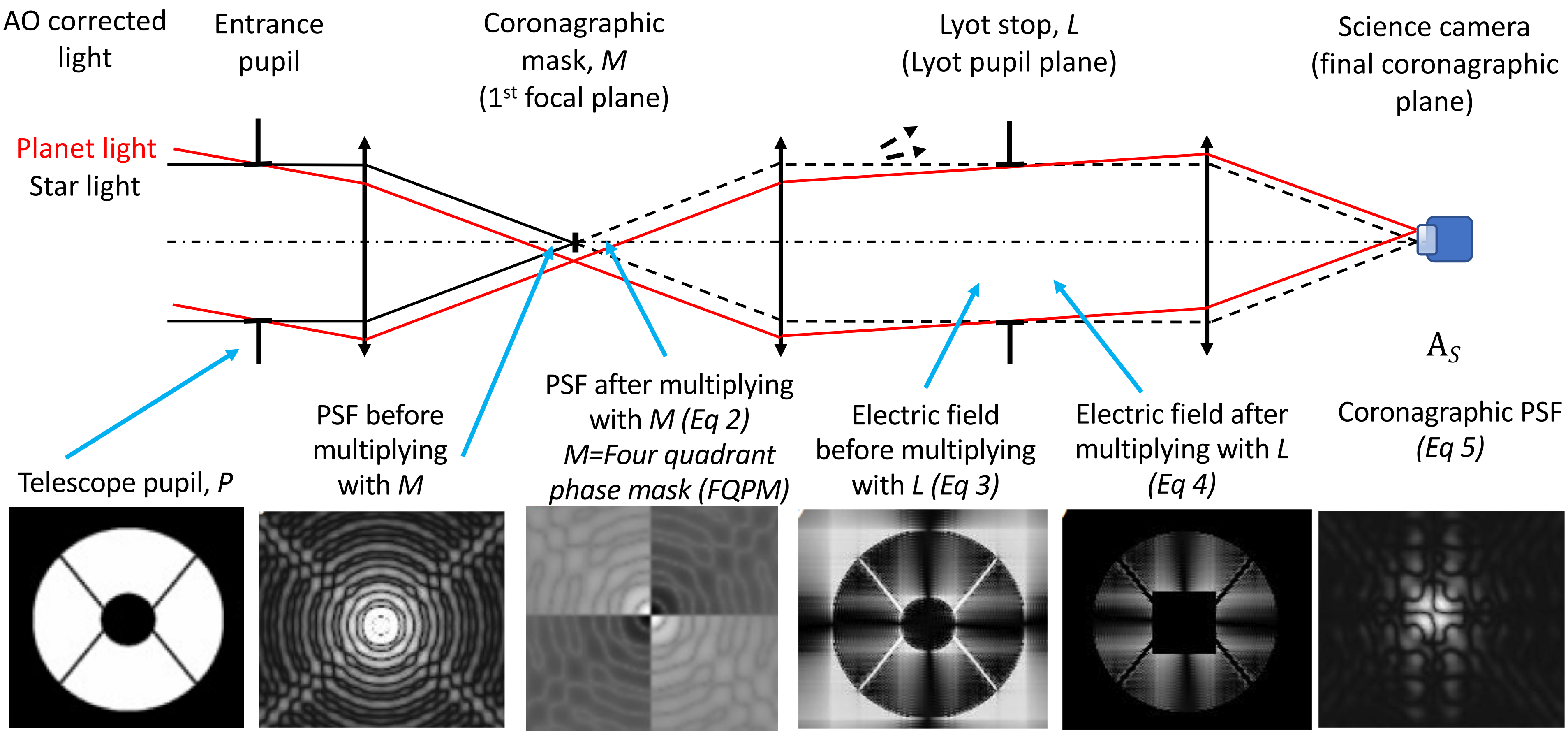

What causes residual aberrations in Exoplanet Imaging?

Low-order aberrations

Causes: Temperature variations, thermal distortions, optical/mechanical vibrations, alignment errors due to telescope motors and chromatic errors.

Effects: Starlight leak around a coronagraphic mask, prevent detection at small angles.

Low-order errors: Leak starlight (Tilt of 0.5 $\frac{\lambda}{D}$ at the entrance of the pupil)

Simulated images with a FQPM coronagraph

Light leaking through the pupil at Lyot plane | Multiply with a Lyot stop | Aberrated coronagraphic PSF

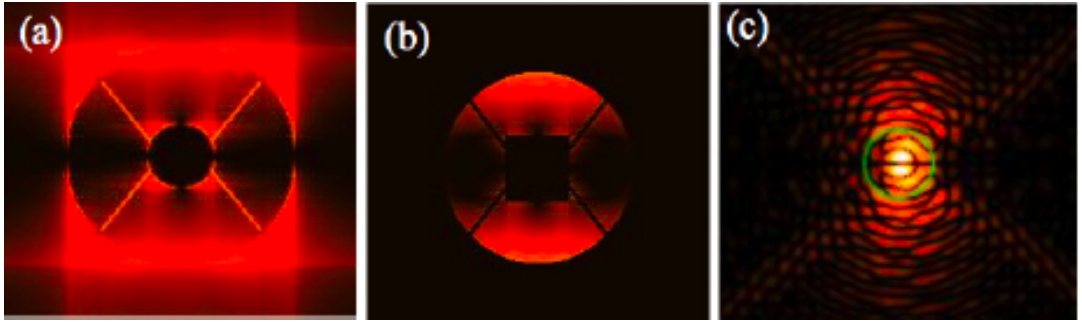

Tip-tilt mimics exoplanet signals.

Focus/astigmatism mimics circumstellar disks features.

Perfectly aligned coronagraphic PSF | coronagraphic PSF with a tilt error | Light leaking through the pupil at Lyot plane

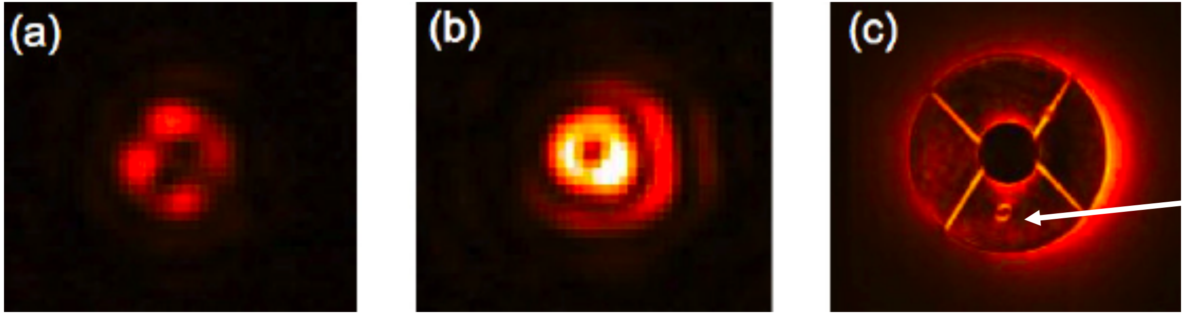

Dead actuator!

Laboratory images of vector vortex coronagraph on SCExAO instrument

*images are not at same brightness scale

Reference: Singh 2015, Thesis “Low-order Wavefront control and calibration for phase mask coronagraphs”

Low-order errors: Coronagraphic low-order wavefront sensor (CLOWFS)

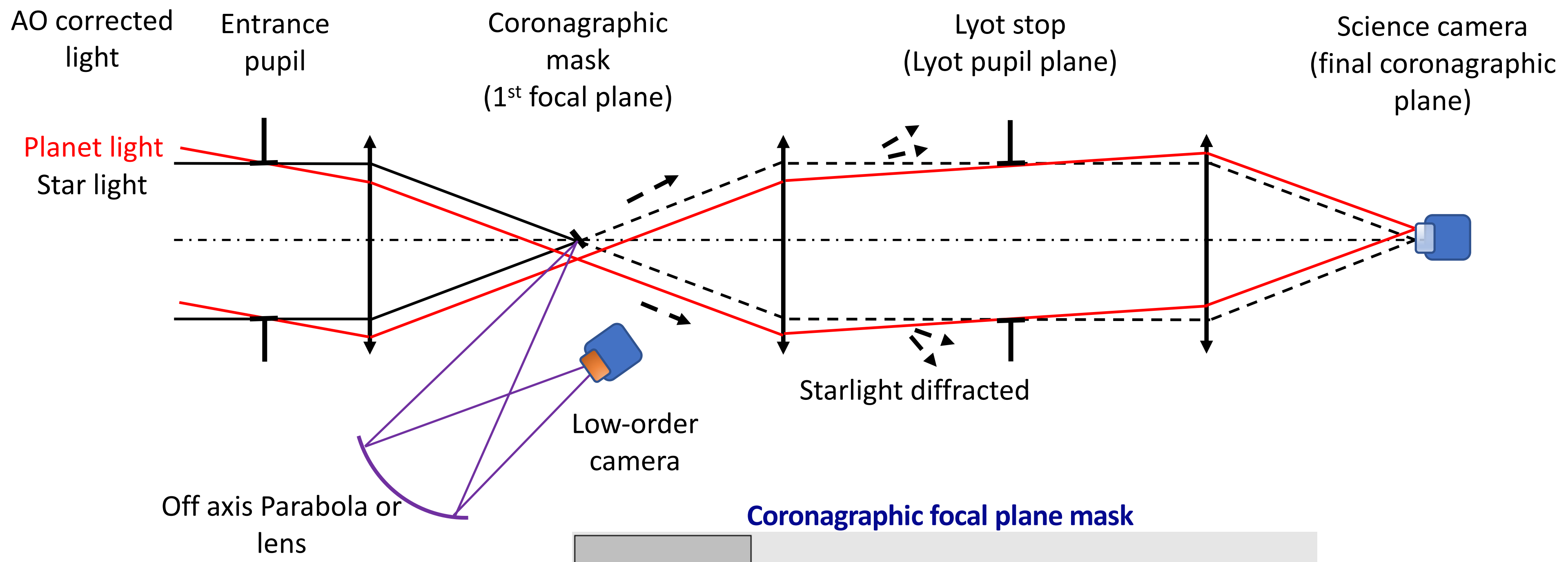

Coronagraphic focal plane mask

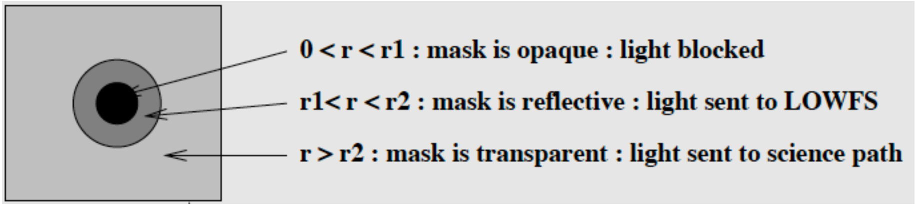

Guyon et al 2009

Low-order errors: Lyot-stop low-order wavefront sensor (LLOWFS)

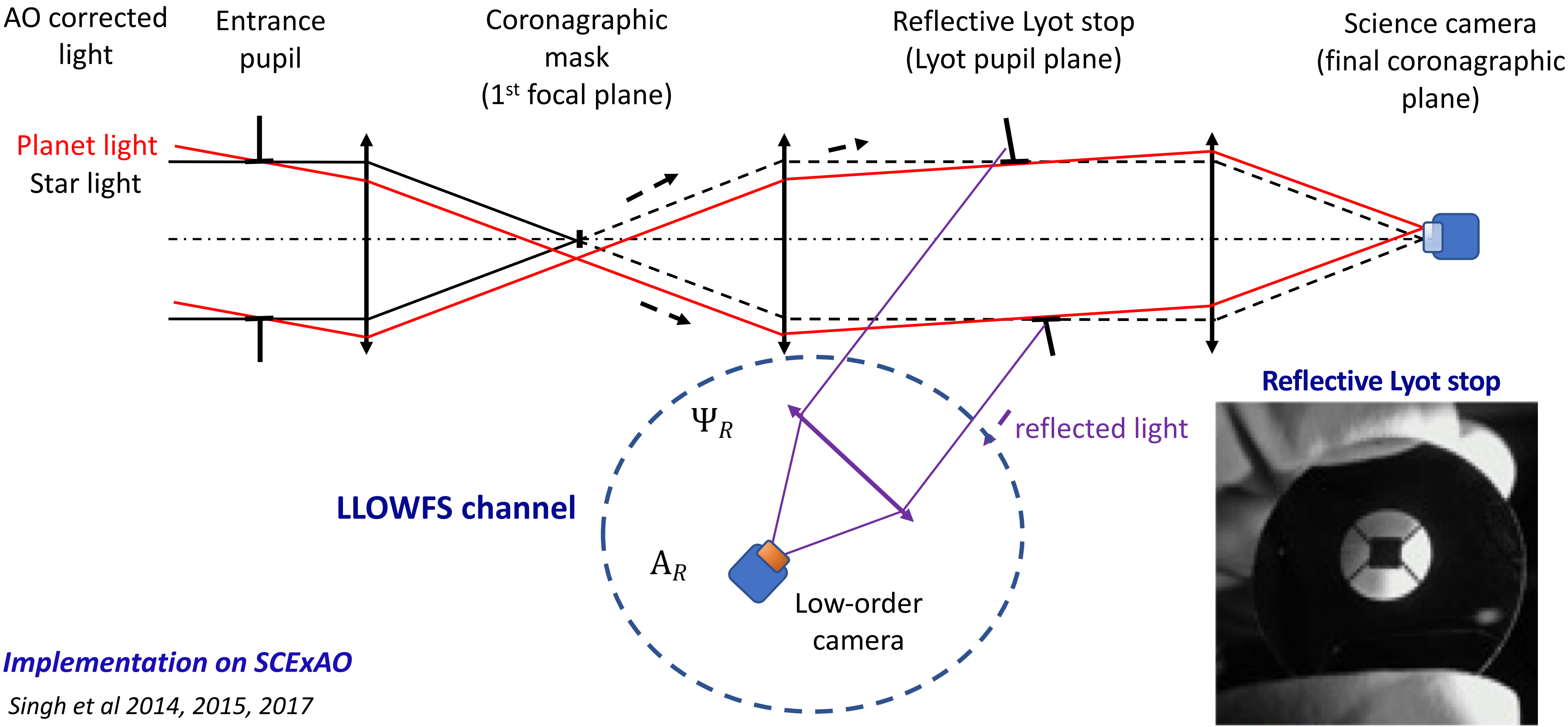

Reflective Lyot stop

Implementation on SCExAO

Singh et al 2014, 2015, 2017

Low-order errors: Principle of both CLOWFS and LLOWFS is same

How does CLOWFS/LLOWFS sense the WF aberrations using the starlight rejected by a coronagraphs?

Lets look at the LLOWFS

The electric field inside the Lyot plane given by Equation 4 is

$$\frac{\psi_S}{\psi_0} = (P * \mathcal{F}^{-1}[M])L + (\Phi * \mathcal{F}^{-1}[M])L \qquad \text{Eq 4}$$

The electric field outside the Lyot plane can be written as

$$\frac{\psi_R(\xi,\lambda)}{\psi_0} = (P * \mathcal{F}^{-1}[M])(1 - L) + i\,(\Phi * \mathcal{F}^{-1}[M])(1 - L) \qquad \text{Eq 6}$$

The complex amplitude at the LLOWFS focal plane ((A_R = $\mathcal{F}(\Psi_R)$) in the LLOWFS channel is

$$\frac{A_R(x)}{\psi_0} = \underbrace{(\mathcal{F}[P]M)}_{A_0} + i\,\underbrace{(\mathcal{F}[\Phi]M) * \mathcal{F}[(1 - L)]}_{G[\Phi]} \qquad \text{Eq 7}$$

LLOWFS Hypothesis

Eq 7 becomes

$$\frac{A_R(x)}{\psi_0} = A_0 + mG[\Phi]$$ Eq 8

A_0 is the complex amplitude obtained by the LLOWFS camera for a perfect wavefront.

Hypothesis is that the complex amplitude distribution A_R in the LLOWFS camera and the change introduced on this complex amplitude by the low-order modes to me measured is nonorthogonal.
Eq 8 is a linear function of Φ

The reflected light intensity at the LLOWFS focal plane is $I_R = |A_R|^2$

$$I_R = I_0 + 2Re[A_0\overline{mG[\phi]}] + |mG[\phi]|^2$$ Eq 9

I_0 is the reflected intensity with no Wavefront aberration. **This is a reference image!**
I_R is a linear function of $G[\Phi]$ as long as

$|mG[\phi]|^2 \ll Re[A_0\overline{mG[\phi]}]$, which is the case with small aberrations!

Eq 9 becomes

$$I_R = I_0 + 2Re[A_0\overline{mG[\phi]}] \qquad \text{Eq 10}$$

This is the basis of LLOWFS/CLOWFS theory!
The variations in I_R is a linear function of the low-order aberrations causing coronagraphic leaks.

A general mathematical expression of the LLOWFS can be written as:

N is the total number of modes

An aberrated image at an instant *t*

$$I_{R(\alpha)} - I_0 = \sum_{i=1}^{n} \alpha_i S_i + \nu_n \qquad \text{Eq 11}$$

Residual of high-order mode

Pre-acquired reference image with no aberrations

Low-order mode *i* of amplitude α

Pre-acquired response of the sensor to low-order mode *i*
(Calibration frames)

$$I_{R(\alpha)} - I_0 = \sum_{i=1}^{n} \alpha_i S_i + \nu_n$$

Any reference subtracted LLOWFS image can be decomposed linearly on a base of orthonormal images S_i corresponding to the response of the sensor to the low-order modes.

Modal reconstruction

Apply a mode *i* of known amplitude α_{ci} and record the response of the sensor:

$$S_i = \frac{I_{Ri} - I_0}{a_{ci}}$$

I_{Ri} is the LLOWFS image recorded for the mode *i*

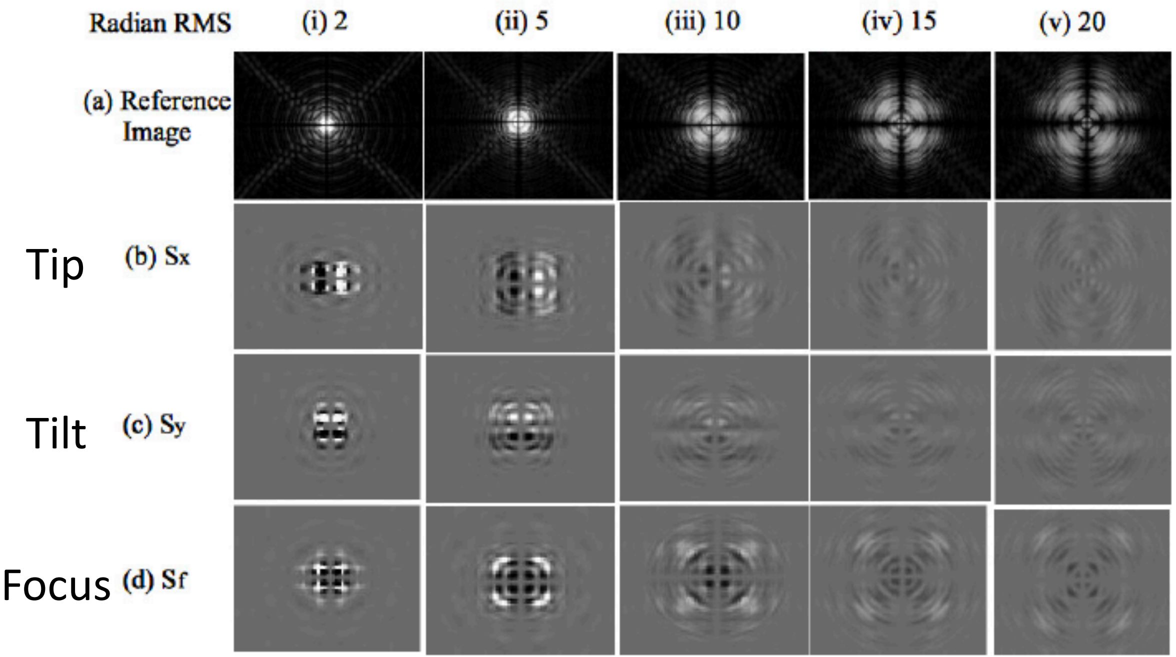

Control loop of the LLOWFS

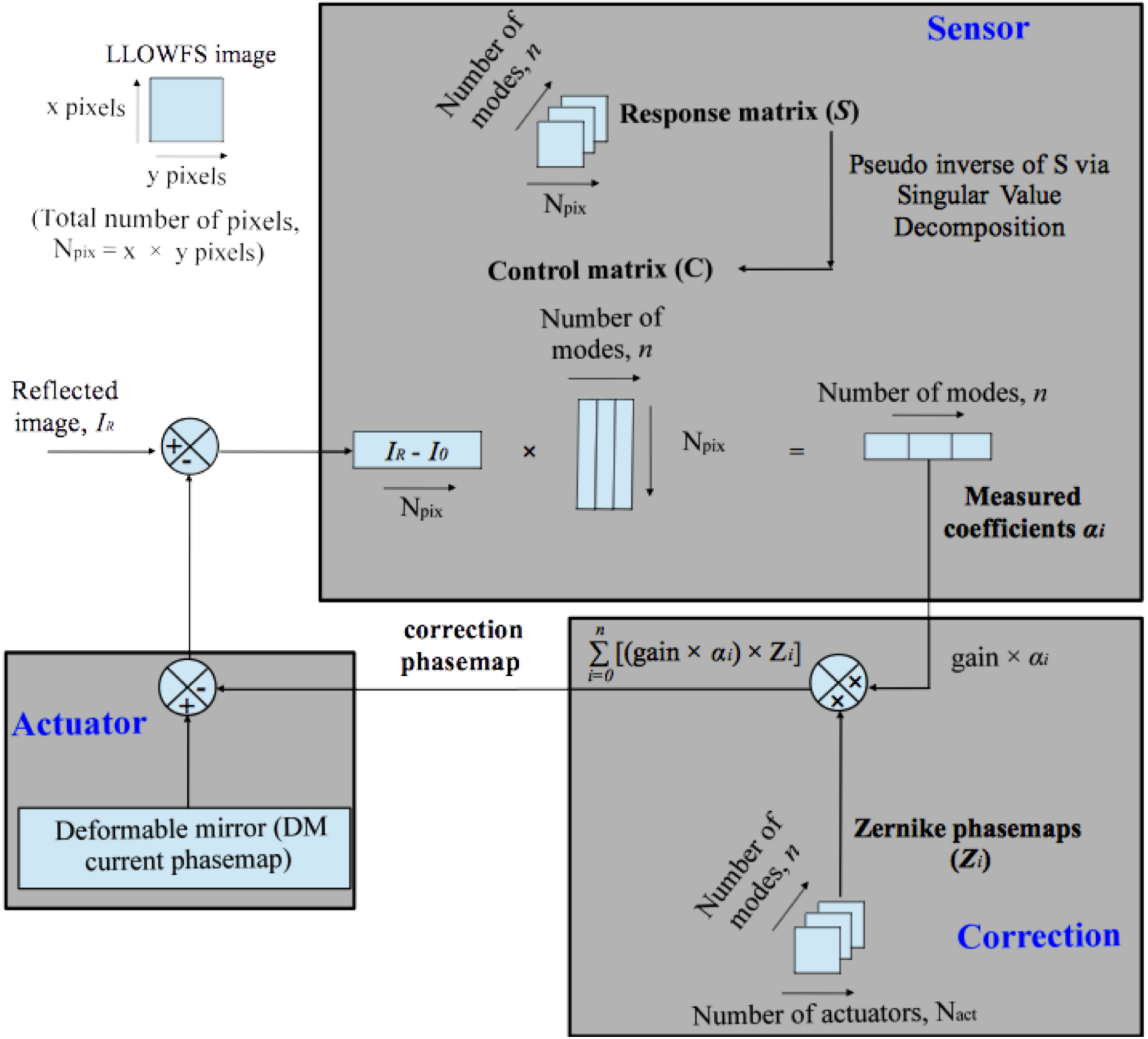

LLOWFS in action

On-sky*, no low-order corrections

On-sky, LLOWFS loop closed on 10 modes

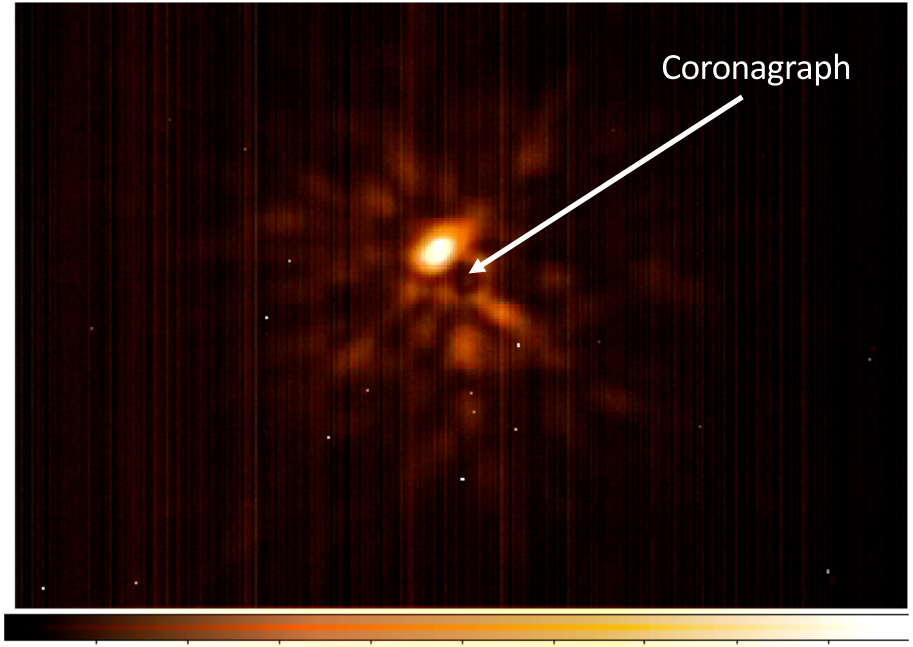

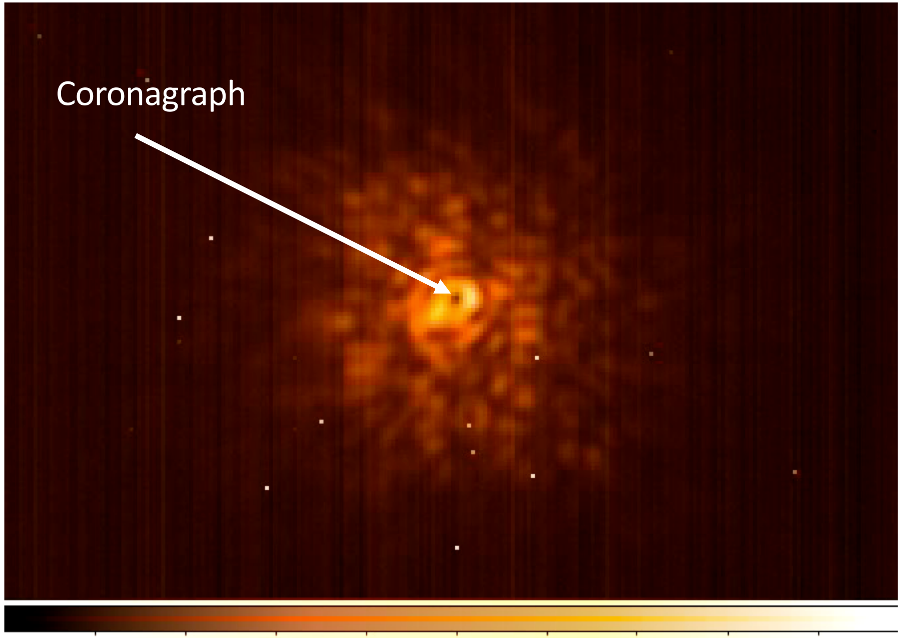

PIAA coronagraph

Vector vortex coronagraph
(Correction at 170 Hz in H band)

Videos from AO188 + SCExAO instrument at Subaru Telescope

*Raw frames with bad pixels and without dark subtracted

What causes residual aberrations in Exoplanet Imaging?

Low-order aberrations

Causes: Temperature variations, thermal distortions, optical/mechanical vibrations, alignment errors due to telescope motors and chromatic errors.

Effects: Starlight leak around a coronagraphic mask, prevent detection at small angles.

Non-common path aberrations (NCPA)

Cause: different AO sensing and science imaging channels.

Effects: Evolving quasi-static stellar speckles, which not only mask faint exoplanet signals but also create false positive signals.

Non common path aberrations: Evolving quasi static speckles

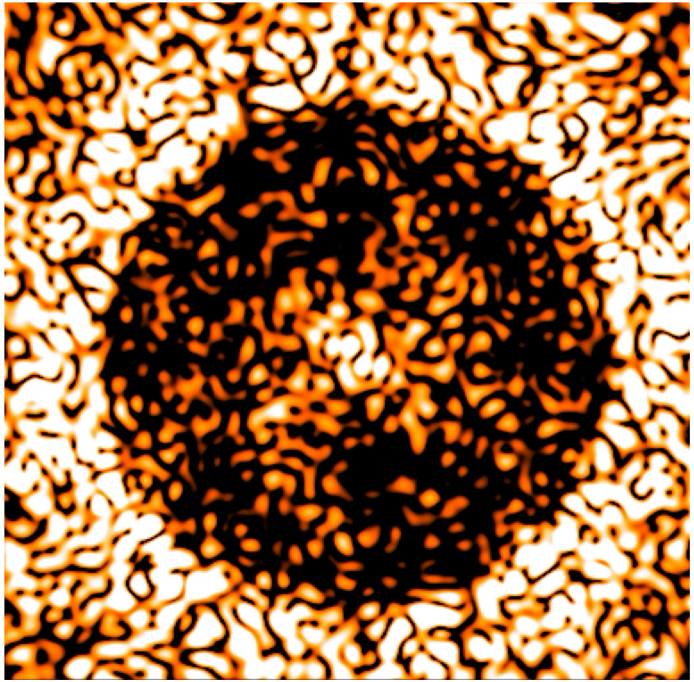

Video consists of short exposure frames acquired in the laboratory on the THD2 bench under the effect of post-AO residuals as seen by the SPHERE instrument at VLT. Coronagraph: FQPM

Long exposure coronagraphic image

=

Smooth halo, created by AO-induced fast varying speckles that average out. Add photon noise on the planet detection.

+

Static speckles with evolution lifetime greater than the time required to acquire a complete sequence of images (typically 30min-1h).

Can be calibrated a posteriori using observing strategies like angular/spectral differential imaging.

+

Quasi-static speckles: vary slowly during the observing sequence.

NCPA that evolve during science acquisition cannot be calibrated, which as a result leave evolving speckles in the images.

Non common path aberrations: Evolving quasi static speckles

How to discriminate speckles of the star from a faint companion during an exposure?

Calibrating slowly drifting quasi static speckles ⟷ Differential imaging techniques

Speckles could be discriminated from planets using:

- Spectrophotometry (Racine et al. 1999, Marois et al. 2005)
- Polarimetry (Seager et al. 2000, Baba & Murakami 2003)
- Coherence (Codona & Angel 2004, Guyon 2004, Labeyrie 2004)

Depends on physical properties of the planets!

Fizeau recombination of the science beam and the reference beam

Non common path aberrations: Focal plane WFS

Lets consider a Fizeau interferometer.
Assume a telescope aperture masked by two small circular subaperutres of diameter < r_0. (Negligible effects of turbulence on the intensity distribution of the beam)

For a monochromatic point source, the superposition of two beams at the detector plane produces interference fringes.

The resulting complex amplitude,

$$\Psi = \Psi_1 + \Psi_2 \,,$$

and the intensity $\mathrm{I} = |\Psi|^2$

$$\mathrm{I} = |\Psi_1|^2 + |\Psi_2|^2 + 2\mathrm{Re}(\Psi_1 \Psi_2^*) \qquad \textbf{Eq 12}$$

* is a complex conjugate

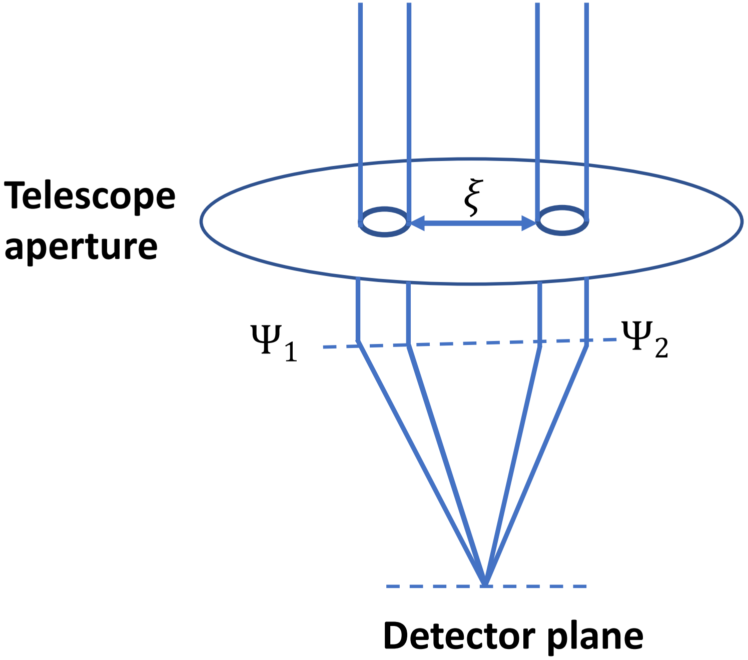

Interference pattern describing a fringe pattern, which is a sinusoidal function

Fringe amplitude = $|\Psi_1 \Psi_2^*|$

Non common path aberrations: Self Coherent Camera as a Focal plane WFS

Requirement:- In a long-exposure image, first measure the quasi-static field above the AO halo and then actively minimize the quasi-static speckles.

Method:- Self coherent camera (SCC) is one such method which measures the electric field associated to the speckles directly from a coronagraphic image *(Baudoz et al 2006, 2012)*. SCC is based on the concept of Fizeau interference.

Non-common path aberrations: Self Coherent Camera (SCC)

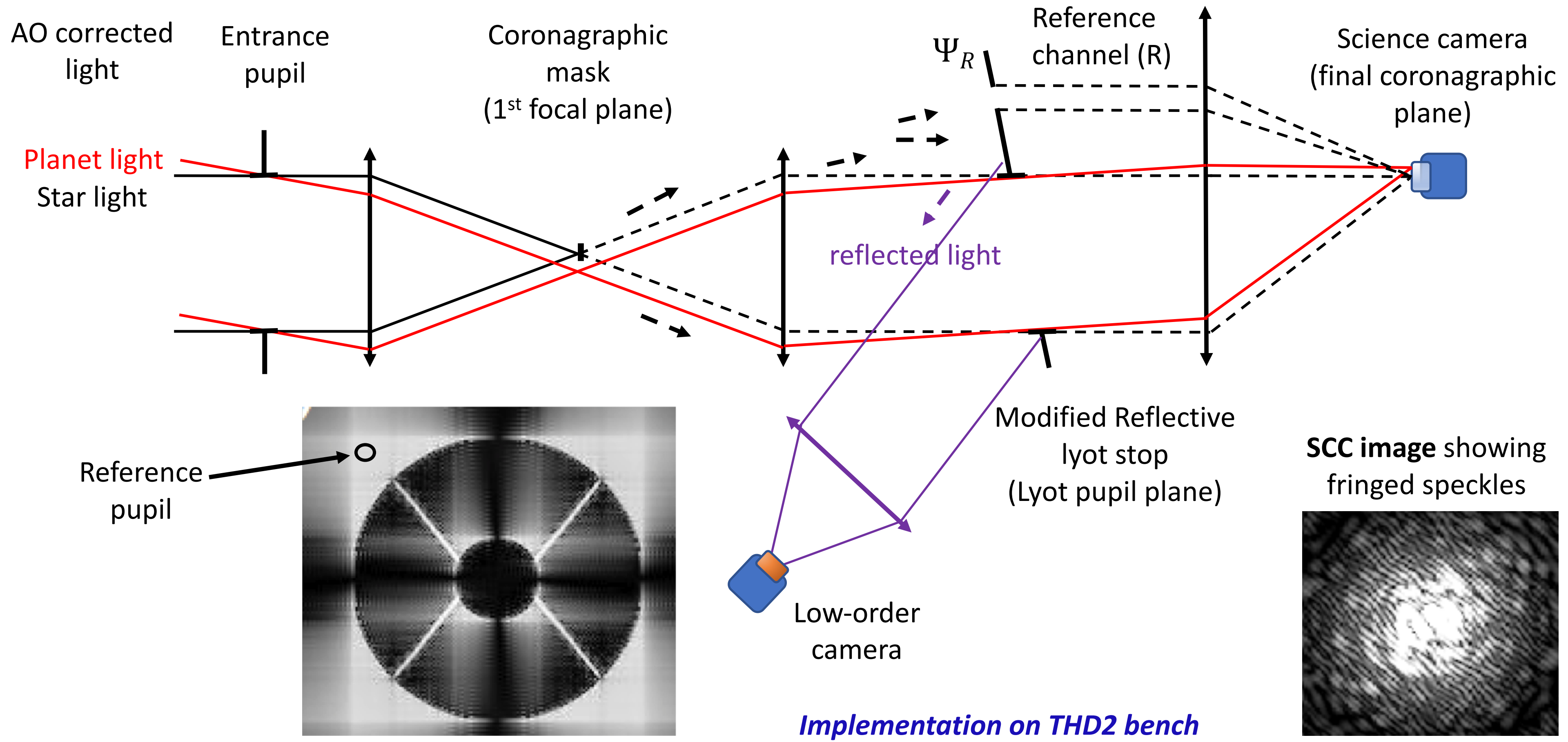

Non-common path aberrations: Self Coherent Camera (SCC)

Requirement:- In a long-exposure image, first measure the quasi-static field above the AO halo and then actively minimize the quasi-static speckles.

Method:- Self coherent camera (SCC) is one such method which measures the electric field associated to the speckles directly from a coronagraphic image *(Baudoz et al 2006, 2012)*. SCC is based on the concept of Fizeau interference. It creates Fizeau fringes in the focal plane, which spatially modulates the speckles.

The electric field ψ after the modified reflective Lyot stop as shown in the previous slide is:

$$\psi(\boldsymbol{\xi}, \lambda) = \psi_S(\boldsymbol{\xi}, \lambda) + \psi_R(\boldsymbol{\xi}, \lambda) * \delta(\boldsymbol{\xi} - \boldsymbol{\xi}_0) \qquad \textbf{Eq 13}$$

ξ_0 is the separation between the two pupils in the modified Lyot stop.
ψ_S is defined in Eq 4.
ψ_R is the complex amplitude in the reference pupil. A_R ($\mathcal{F}(\Psi_R)$) is the complex amplitude in the focal plane, of the light issued from the reference pupil *R*.

Non-common path aberrations: Self Coherent Camera (SCC)

The final intensity ($I = |\mathcal{F}(\Psi)|^2$) at the focal plane on the detector can be written as:

$$I(\boldsymbol{x}) = |A_S(\boldsymbol{x})|^2 + |A_R(\boldsymbol{x})|^2 + A_S^*(\boldsymbol{x})\, A_R(\boldsymbol{x}) \exp\left(\frac{-2i\pi \boldsymbol{x}.\boldsymbol{\xi}_0}{\lambda}\right) + A_S(\boldsymbol{x})\, A_R^*(\boldsymbol{x}) \exp\left(\frac{2i\pi \boldsymbol{x}.\boldsymbol{\xi}_0}{\lambda}\right),$$

Eq 14

SCC image

These correlation terms creating fringes directly depends on A_R and A_S

See references to look for more details on SCC (Equations are taken from Mazoyer et al., 2013, A&A 557, A9)

Non-common path aberrations: Self Coherent Camera (SCC)

Now measure complex amplitude of the speckle field. Take inverse Fourier transformation of I

I_1

$$\mathcal{F}^{-1}[I](u) = \mathcal{F}^{-1}[I_S + I_R] + \mathcal{F}^{-1}[A_S^* A_R] * \delta\left(u - \frac{\xi_0}{\lambda}\right)$$
$$+ \mathcal{F}^{-1}[A_S A_R^*] * \delta\left(u + \frac{\xi_0}{\lambda}\right),$$

I_-

Lateral peaks has the information on the complex amplitude of the stellar speckles that are spatially modulated on the detector

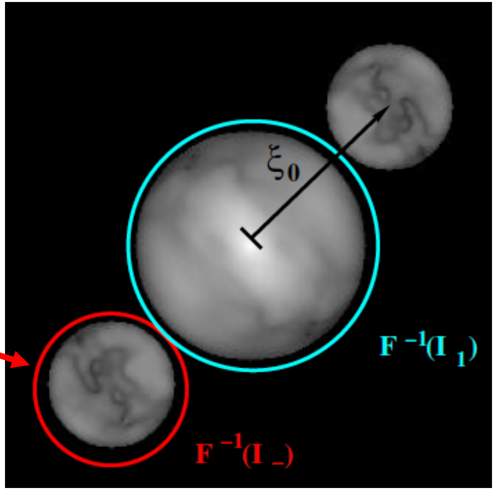

Correlation peaks in the $\mathcal{F}^{-1}[I]$

Retrived per image

$$\mathcal{F}^{-1}[I_-] = \mathcal{F}^{-1}[A_S A_R^*] \longleftrightarrow A_S = \frac{I_-}{A_R^*}. \xleftrightarrow{\text{Equating } A_S \text{ in Eq 5}} \Phi_{\text{est}} = \left[i\mathcal{F}^{-1}\left[\frac{I_-}{A_R^* \psi_0 M}\right]\right] P.$$

Can be measured in the lab

This is it!

Active minimization of non common path aberrations

THD2 bench, Observatory of Paris
http://thd-bench.lesia.obspm.fr/

Phase errors: Dynamically changing post-AO phase residuals at the entrance pupil of SPHERE/VLT. Standard deviation of the phase errors ~ 40 nm. Both phase and amplitude static errors were also applied on two DMs (5 nm rms of phase and 0.4% of amplitude).

Movie clip showing active correction of speckles, creating a 25 x 25 λ/D dark hole in 5 iterations. Each frame/image/iteration is a long exposure image acquired at 18s exposure.

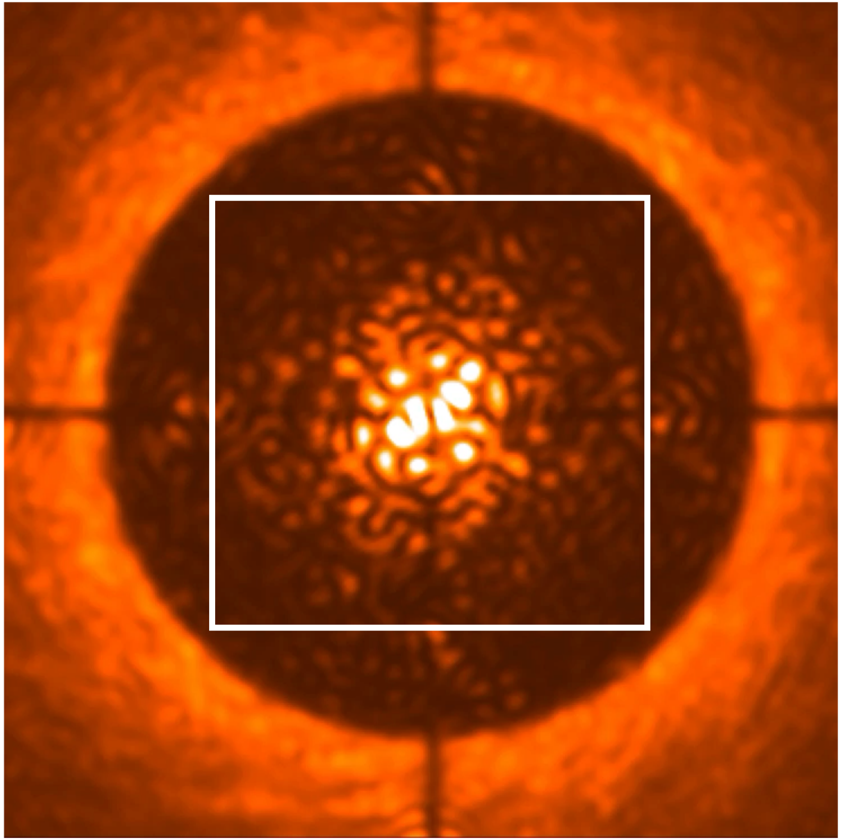

0th iteration

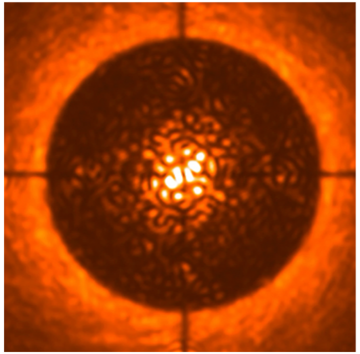

5th iteration

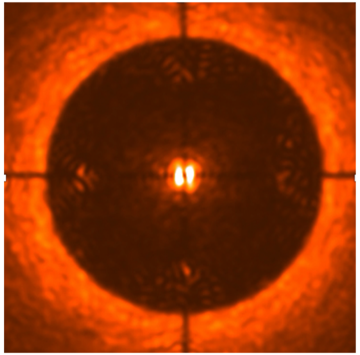

Singh et al 2019, "*Active minimization of non-common path aberrations in long-exposure imaging of exoplanetary systems»* Submitted A&A

What causes residual aberrations in Exoplanet Imaging?

Low-order aberrations

Causes: Temperature variations, thermal distortions, optical/mechanical vibrations, alignment errors due to telescope motors and chromatic errors.

Effects: Starlight leak around a coronagraphic mask, prevent detection at small angles.

Non-common path aberrations (NCPA)

Cause: different AO sensing and science imaging channels.

Effects: Evolving quasi-static stellar speckles, which not only mask faint exoplanet signals but also create false positive signals.

Low-wind effect

Cause: Spider arms of the secondary can cool below the ambient air temperature due to radiative losses. Change in air index from one side of the spider to the other.

Effects: Each quarter of the pupil shows different piston and sometimes tip-tilt phase errors.

Low-wind effect

**More details can be found in Sauvage et al 2015*

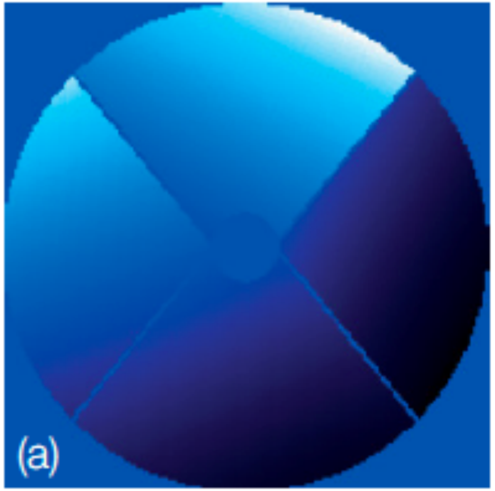

Differential tip-tilt phase map due to low wind effect

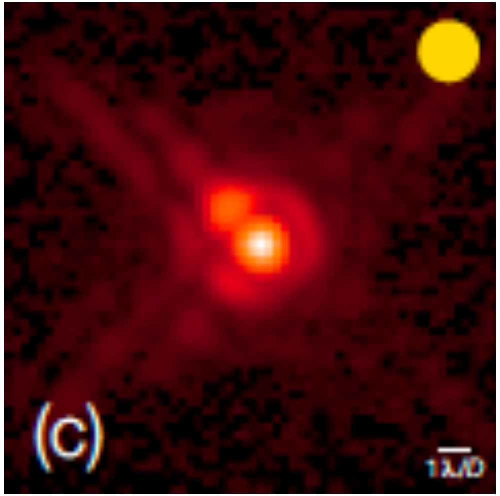

Non coronagraphic on-sky PSF at VLT

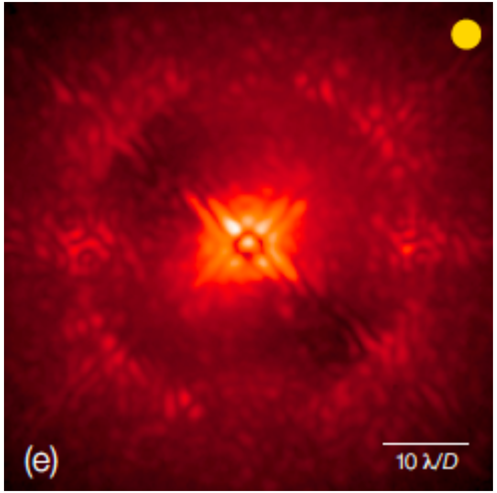

coronagraphic on-sky PSF where low wind effect dominates

SHWFS is insensitive to phase steps! To reduce this effect, the spiders of secondary at VLT is covered with low emissivity coating to prevent radiative cooling. This effect has been reduced from 18% to 3%. (Milli et al 2018.)

Figure 11 taken from Cantalloube et al. 2019 – Peering through SPHERE images: A glace at contrast limitations

What causes residual aberrations in Exoplanet Imaging?

Low-order aberrations

Causes: Temperature variations, thermal distortions, optical/mechanical vibrations, alignment errors due to telescope motors and chromatic errors.

Effects: Starlight leak around a coronagraphic mask, prevent detection at small angles.

Non-common path aberrations (NCPA)

Cause: different AO sensing and science imaging channels.

Effects: Evolving quasi-static stellar speckles, which not only mask faint exoplanet signals but also create false positive signals.

Low-wind effect

Cause: Spider arms of the secondary can cool below the ambient air temperature due to radiative losses. Change in air index from one side of the spider to the other.

Effects: Each quarter of the pupil shows different piston and sometimes tip-tilt phase errors.

Wind driven halo

Cause: High wind speeds at the upper level of turbulence across the pupil moving faster then the speed of AO loop correction.

Effects: A typical butterfly-shaped structure in the focal plane image along the wind direction.

Wind-driven Halo

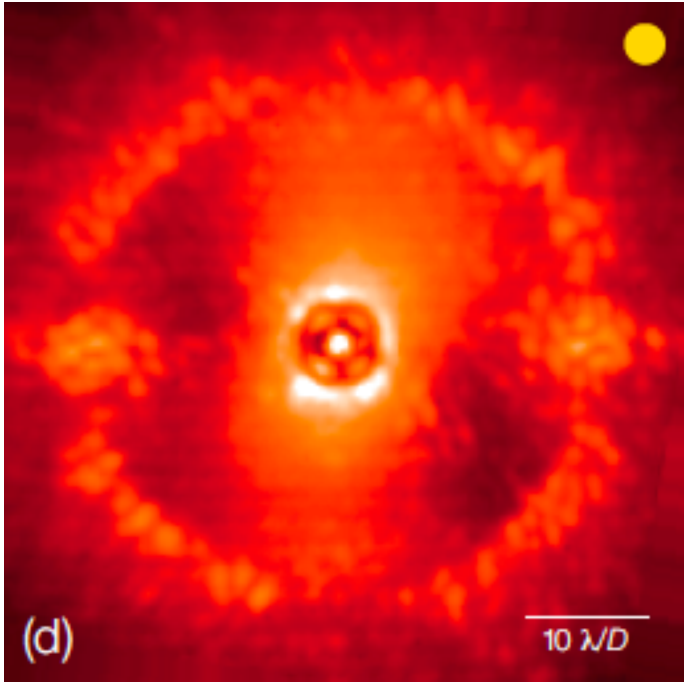

coronagraphic on-sky PSF where wind driven halo dominates

Fast moving (~ 50 m/s) high altitude jet stream atmospheric layer (located at ~12 km above paranal) causes wind driven halo in VLT images.

An asymmetry in this pattern is also observed due to interference between this temporal lag error and scintillation errors.

**More details can be found in Mouillet et al 2018, Madurowicz et al. 2018 and Cantalloube et al 2018*

Figure 9 taken from Cantalloube et al. 2019 – Peering through SPHERE images: A glace at contrast limitations

References

Revisiting WFSs
https://pdfs.semanticscholar.org/bd9c/7d0129ba8944c2e98cd00edf7d5a4e3cf8b1.pdf

PyWFS: Ragazzoni 1996
http://www.mpia.de/AO/INSTRUMENTS/PYRAMIR/DOCS/RagazzoniJModOptics1996.pdf

Fourier reconstruction
Poyneer, L. A., Gavel, D. T., and Brase, J. M. “Fast Wave-Front Reconstruction in Large Adaptive Optics Systems with Use of the Fourier Transform” Journal of the Optical Society of America A: Optics and Image Science, and Vision 19, no. 10 (2002):

SCC
Baudoz, P., Boccaletti, A., Baudrand, J., & Rouan, D. 2006, in IAU Colloq. 200: Direct Imaging of Exoplanets: Science & Techniques, ed. C. Aime & F. Vakili, 553–558
Baudoz, P., Mazoyer, J., Mas, M., Galicher, R., & Rousset, G. 2012, in Proc. SPIE, Vol. 8446, Ground-based and Airborne Instrumentation for Astronomy IV, 84468C
Galicher, R., Baudoz, P., Rousset, G., Totems, J., & Mas, M. 2010, A&A, 509,A31
Mazoyer, J., Baudoz, P., Galicher, R., & Rousset, G. 2014, A&A, 564, L1

CLOWFS
Guyon, O., Matsuo, T., & Angel, R. 2009, ApJ, 693, 75
Vogt, F. P. A., Martinache, F., Guyon, O., et al. 2011, PASP, 123, 1434

LLOWFS
Singh, G., Martinache, F., Baudoz, P., et al. 2014, PASP, 126, 586
Singh, G., Lozi, J., Jovanovic, N., et al. 2017, PASP, 129, 095002
Garima Singh, Thesis 2015, titled « Low-order wavefront control and calibration for phase mask coronagraphs»